

RESEARCH PAPER



Molecular design, synthesis and *in vitro* biological evaluation of thienopyrimidine–hydroxamic acids as chimeric kinase HDAC inhibitors: a challenging approach to combat cancer

Mona M. Abdel-Atty^a, Nahla A. Farag^a, Rabah A. T. Serya^b, Khaled A. M. Abouzid^{b,c} and Samar Mowafy^{a,d}

^aPharmaceutical Chemistry Department, Faculty of Pharmacy, Misr International University, Cairo, Egypt; ^bPharmaceutical Chemistry Department, Faculty of Pharmacy, Ain Shams University, Cairo, Egypt; ^cOrganic and Medicinal Chemistry Department, Faculty of Pharmacy, University of Sadat City, Sadat City, Egypt; ^dDepartment of Chemistry, University of Washington, Seattle, WA, USA

ABSTRACT

A series of thieno[2,3-*d*]pyrimidine-based hydroxamic acid hybrids was designed and synthesised as multi-target anti-cancer agents, through incorporating the pharmacophore of EGFR, VEGFR2 into the inhibitory functionality of HDAC6. Three compounds (**12c**, **15b** and **20b**) were promising hits, whereas (**12c**) exhibited potent VEGFR2 inhibition ($IC_{50}=185$ nM), potent EGFR inhibition ($IC_{50}=1.14$ μ M), and mild HDAC6 inhibition (23% inhibition). Moreover, compound (**15c**) was the most potent dual inhibitor among all the synthesised compounds, as it exhibited potent EGFR and VEGFR2 inhibition ($IC_{50}=19$ nM) and ($IC_{50}=5.58$ μ M), respectively. While compounds (**20d**) and (**7c**) displayed nanomolar selective kinase inhibition with EGFR $IC_{50}=68$ nM and VEGFR2 $IC_{50}=191$ nM, respectively. All of the synthesised compounds were screened *in vitro* for their cytotoxic effect on 60 human NCI tumour cell lines. Additionally, molecular docking studies and ADMET studies were carried out to gain further insight into their binding mode and predict the pharmacokinetic properties of all the synthesised inhibitors.

ARTICLE HISTORY

Received 6 March 2021
Revised 13 May 2021
Accepted 14 May 2021

KEYWORDS

Thieno[2,3-*d*]pyrimidine; hydroxamic acid derivatives; chimeric HDAC-kinase inhibitors; multitarget therapy lead; ADMET study

1. Introduction


The development of multitarget drug therapy has become an important strategy for cancer treatment. Recently, the modulation of receptor tyrosine kinase (RTK) pathways by the inhibition of histone deacetylases (HDACs) has become a promising approach for cancer therapy¹. HDACs are a family of numerous epigenetic enzymes that are important therapeutic targets for cancer². HDACs have been classified into four distinct classes, in which class I (HDAC1–3 and 8), class II (HDAC4–7, 9 and 10), and class IV (HDAC11)³. HDAC6 is considered a therapeutically important target for cancer treatment due to its interaction with proteins involved in cell growth, migration, protein degradation, and apoptosis⁴. It is reported that HDAC inhibitors with large or rigid hydrophobic surface recognition moiety (SRM) and bulky aromatic or short linkers, are more efficient to achieve HDAC6 selectivity, which could achieve a closer approach of the hydroxamate group to Zn²⁺⁵. Numerous HDAC6 inhibitors have been developed having large SRM connected to the zinc-binding group (ZBG) with diverse linkers (Figure 1)^{5–7}.

Despite the efficiency of HDAC inhibition as monotherapy in haematologic malignancies, it did not show significant competency against solid tumours. As a result, multitarget therapy is developed as a challenging approach for increasing the efficacy of HDAC inhibitors⁸. The combination of HDAC and TKIs is considered a promising approach to enhance therapeutic effect and repress resistance¹. For example, a synergistic effect is observed

by a combination of gefitinib (EGFR inhibitor) with vorinostat (HDAC inhibitor) by enhancing tumour growth inhibition and apoptosis compared with monotherapy of selective EGFR inhibitors^{9,10}. Another example, combination therapy of pazopanib (VEGFR2 inhibitor) and abexinostat (HDAC inhibitor) showed that HDAC inhibition could improve response and holdback resistance to pazopanib in patients with solid tumour malignancies and renal cell carcinoma¹¹. Thus, it is suggested that a single molecule that simultaneously inhibits HDAC and RTK activities targeting multiple biological molecules and multiple signal pathways can not only enhance drug efficacy but also can have additive or even synergistic antitumor effects and can overcome the problems of cancer resistance and relapse. Additionally, it can overcome unfavourable pharmacokinetic properties, drug–drug interactions, poor patient compliance, and high drug cost involved in multicomponent drug cocktails^{1,12}. CUDC-101 is a first-in-class multi-targeted hybrid that was designed to simultaneously inhibit HDACs, EGFR, and HER2. It was found that it induces significantly synergistic tumour regression in breast, NSCLC, liver, colon, head, neck, and pancreatic cancers¹. Series of hybrids of 4-anilinoquinazoline based hydroxamic acid derivatives were synthesised and discovered as dual VEGFR-2/HDAC inhibitors and EGFR/HDAC inhibitors (Figure 2)^{13,14}.

Moreover, the development of dual-inhibitors targeting EGFR and VEGFR2 has recently become a promising strategy for the treatment of diverse types of cancer to overcome problematic drug resistance and low response to selective tyrosine kinase inhibitors (TKIs) and to produce a synergistic effect¹⁵. Inhibition of

CONTACT Samar Mowafy  samarmowafy@gmail.com, khaled.abouzid@pharma.asu.edu.eg Pharmaceutical Chemistry Department, Faculty of Pharmacy, Misr International University, Cairo, Egypt

 Supplemental data for this article can be accessed [here](#).

© 2021 The Author(s). Published by Informa UK Limited, trading as Taylor & Francis Group.

This is an Open Access article distributed under the terms of the Creative Commons Attribution License (<http://creativecommons.org/licenses/by/4.0/>), which permits unrestricted use, distribution, and reproduction in any medium, provided the original work is properly cited.

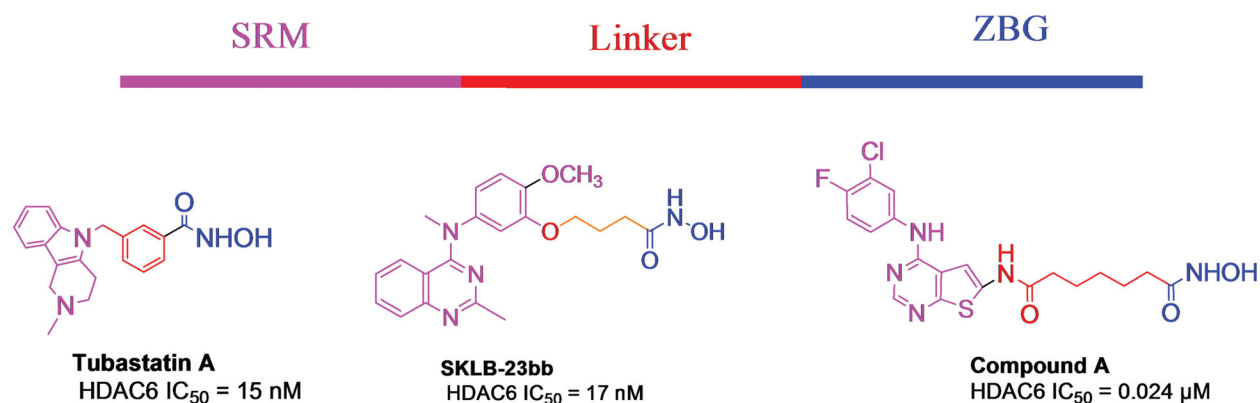


Figure 1. The structures of histone deacetylase 6 (HDAC6) inhibitors, colour codes show essential pharmacophore for HDAC inhibitors composed of zinc-binding group (blue), linker (red), and SRM (purple).

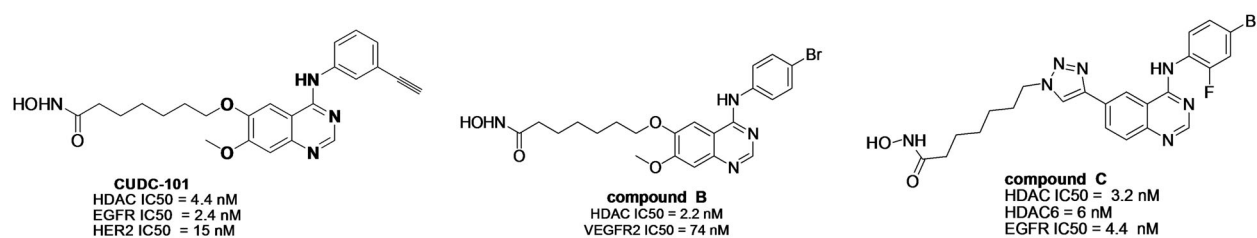


Figure 2. The structures of several reported dual inhibitors HDAC/EGFR or VEGFR2.

both EGFR and VEGFR2 produces a more significant effect on angiogenesis than selective VEGFR2 inhibitors, where EGFR-induced the production of angiogenic growth factors, which indirectly affects angiogenesis^{16,17}. Several EGFR/VEGFR-2 dual inhibitors have been designed and synthesised (Figure 3)^{15,16}.

In this study, six novel series of thieno[2,3-*d*]pyrimidine-based hydroxamic acid derivatives were rationally designed. The design is based on the strategy of multitarget drug therapy and the clinical advantage of combining HDAC, VEGFR2, or/and EGFR inhibition in one single drug. Investigating the structural requirements of EGFR, VEGFR2, and HDAC inhibitors led us to design several series of novel leads of multitarget or dual-target inhibitors by combining the pharmacophore of EGFR, VEGFR2 inhibitors with that of HDAC inhibitors.

2. Rationale of the design

Design strategy is based on the study of several reported dual inhibitors such as CUDC101 and compound B, which were reported as dual EGFR/HDAC and VEGFR2/HDAC inhibitors respectively; (bearing 4-anilinoquinazolinone fragment) (Figure 2)^{14,18}. Additionally, novel dual EGFR/VEGFR2 inhibitors such as compound D and compound E; (bearing thieno[2,3-*d*] pyrimidine fragment); were recently reported (Figure 3)¹⁵.

Based on these reported dual inhibitors and by investigating the structural requirements for EGFR, VEGFR2, and HDAC inhibition, we designed six series of hybrid molecules (**7**, **11**, **12**, **15**, **19** and **20**) with potent multi acting EGFR/VEGFR/HDAC inhibition in an attempt to synergise inhibitory activity, decrease resistance and relapse caused by single-target therapy and also avoid multi-component drug cocktails therapy.

The design aimed at replacing the quinazolinone fragment in CUDC101 and compound B with thieno[2,3-*d*]pyrimidine fragment

as in compound D and compound E, representing SRM of HDAC inhibitors and also showing suitable interactions in the hinge region of ATP-binding site of EGFR and VEGFR2 (Figure 4). This bioisostere replacement is also supported by recent reports of novel HDAC inhibitors bearing thieno[2,3-*d*]pyrimidine fragments representing the SRM that displayed excellent inhibitory activities on HDACs, such as compound A as shown in (Figure 1)⁷. Addition of aniline, 5-aminobenzimidazole, (4-phenylthioureido)phenylamine and (4-phenylureido)phenylamine fragments to 4-thieno[2,3-*d*]pyrimidine ring will extend the structure to the hydrophobic pocket of EGFR and VEGFR2 (Figure 4). Next, a hydroxamic acid functionality was directly attached to the thieno[2,3-*d*]pyrimidine fragment (SRM) or connected with a short linker through a connecting amide unit as the previously reported HDAC6 inhibitors (Figure 1)^{19,20}, in which it served as a bridge to properly display HDAC6 inhibitory pharmacophore features and the solvent-accessible area of EGFR- and VEGFR2-binding sites (Figure 4).

3. Results and discussion

3.1. Chemistry

The route adopted for the synthesis of key intermediates (**3**) and (**5a-d**) were prepared according to literature as illustrated in (Schemes 1 and 2), respectively. The synthetic route of the first three series of the target novel hydroxamic acid derivatives with different urea and thiourea moieties (**7a-d**, **11a-c**, **12a-c**) is depicted in (Scheme 3). Moreover, the synthesis of another three series of the novel target hydroxamic acid derivatives with different aniline moieties (**15a-d**, **19b-d**, **20b-d**) is depicted in (Scheme 4).

In (Scheme 1), intermediate (**1**) was synthesised by applying the Gewald reaction, in which ethyl cyanoacetate, ethyl acetoacetate, and sulphur were dissolved in absolute ethanol in the presence of morpholine²¹. The cyclisation of (**1**) into (**2**) was achieved through refluxing (**1**) in a mixture of formamide and acetic acid for 40 h. The structure was confirmed by its reported melting point. Compound (**3**) was synthesised through chlorination of (**2**) by refluxing it with phosphorus oxychloride for 3 h²², (Scheme 1).

The synthesis of the intermediates (**4a-d**) was carried out by reacting the appropriate isocyanate with p-nitroaniline in dry dichloromethane for 48 h at room temperature²³ to yield compounds (**4a-d**), which are then reduced to their corresponding amino derivatives (**5a-d**) using 10% Pd-C in methanol²⁴, (Scheme 2).

In (Scheme 3), the synthesised key intermediates (**5a-d**) were then coupled with the previously prepared chloro derivative (**3**)²⁵ to yield (**6a-d**). The first novel series of the target hydroxamic acid derivatives (**7a-d**) was obtained through the reaction of the ethyl ester group in compounds (**6a-d**) with freshly prepared hydroxylamine in absolute ethanol to give (**7a-d**)^{26,27}, (Scheme 3). Compounds (**7a-d**) were confirmed by many spectral data, in which ¹HNMR signals were consistent with protons of the targeted compounds (**7a-d**). ¹HNMR signals revealed equally integrated signals between δ 8.23–9.82 ppm representing D₂O exchangeable protons of the NH linker, the urea protons, and the NH of hydroxamic acid moiety in all target compounds (**7a-d**). Noticeably, ¹HNMR signals revealed the absence of the triplet and the quartette peak around δ 1.31–1.36 ppm and δ 4.30–4.38 ppm, which confirms the absence of the ester group and the entrance of hydroxamic acid moiety.

Moreover, the synthesis of another two novel series of hydroxamic acid derivatives with urea and thiourea moieties (**11a-c** and **12a-c**) was depicted in (Scheme 3), through multistep reactions. The synthesis starts with the hydrolysis of the carboxylate ethyl ester of the previously prepared compounds (**6a-c**) (Scheme 3), through refluxing it with Li(OH)₂ in THF and water to prepare the intermediate carboxylic acid derivatives (**8a-c**)²⁸. Furthermore, the synthesis of novel two series of intermediate ethyl ester derivatives (**9a-c**, **10a-c**) (Scheme 3) was achieved through coupling of the previously prepared carboxylic acid derivatives (**8a-c**) with the

appropriate amino acid ester hydrochloride salt, utilising EDCI with HOBT in dry DMF²⁹. This method offered a high yield of novel intermediate compounds (**9a-c** and **10a-c**) confirmed by many spectral data. ¹HNMR signals confirmed the prepared structures of the novel esters, in which the aliphatic protons were shown as quartette signals for synthesised novel esters, where it appeared around δ 4.05–4.25 ppm representing the two protons of OCH₂-CH₃ with $J=8$ Hz. Another quartette signal around δ 3.26–3.78 ppm appeared in all compounds referring to two protons of CH₂-NH with $J=8$ Hz. Triplet signal appeared around δ 2.36–2.71 ppm for all compounds, representing the two protons of CH₂-CO with $J=8$ Hz. Moreover, another triplet signal appeared for all compounds around δ 1.17–1.34 ppm, representing three protons of OCH₂-CH₃ with $J=8$ Hz. An additional multiplet signal appeared around δ 1.76–2.04 ppm, representing two protons of CH₂-CH₂-CH₂ in all prepared ethyl ester derivatives of series (**10a-c**) (Scheme 3).

Finally, the ethyl ester group in the previously prepared novel compounds (**9a-c**, **10a-c**) reacted with freshly prepared hydroxylamine in absolute ethanol to obtain target novel hydroxamic acid derivatives (**11a-c**, **12a-c**) (Scheme 3). The two target novel series (**11a-c**, **12a-c**) were confirmed by many spectral data, where ¹HNMR spectrum revealed the disappearance of the quartette signal of the two protons of OCH₂-CH₃ around δ 4.05–4.25 and the triplet signal of the three protons OCH₂-CH₃ around δ 1.17–1.34 ppm, in which it confirms the absence of the ester group and the entrance of the hydroxamic acid moiety.

In (Scheme 4), the purchased compound (5-nitrobenzimidazole) was reduced to afford the corresponding amino derivative (**13a**) using 10% Pd-C in methanol. Prepared compound (**13a**) and purchased aniline derivatives (**13b-d**) were also coupled with the previously prepared chloro derivative (**3**) to give the corresponding thieno[2,3-*d*]pyrimidine derivatives bearing aniline moieties (**14a-d**) (Scheme 4). Finally, the route adopted for the synthesis of the three target novel series of hydroxamic acid derivatives bearing aniline moiety (**15a-d**, **19b-d** and **20b-d**) (Scheme 4) is the same route depicted in (Scheme 3) with the same reagents and conditions. The first novel series of the target hydroxamic acid derivatives (**15a-d**) was obtained through the reaction of the ethyl ester group in compounds (**14a-d**) with freshly prepared

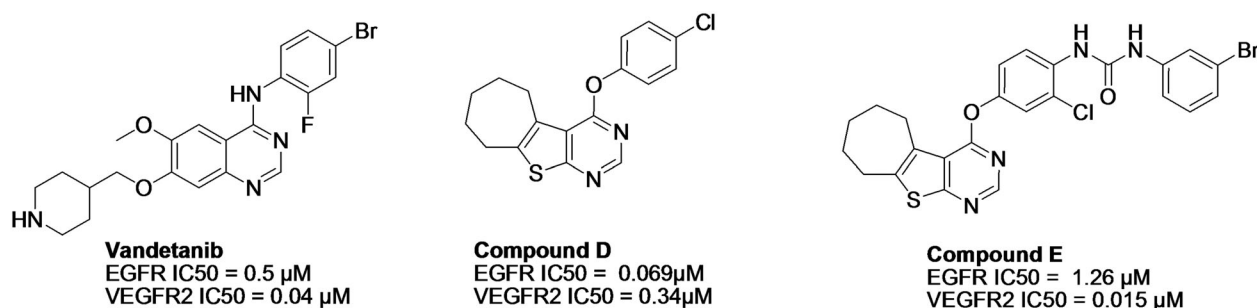
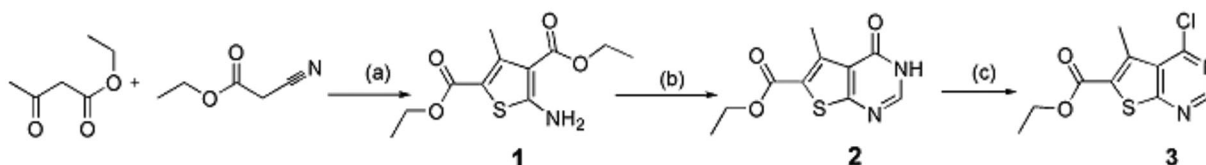
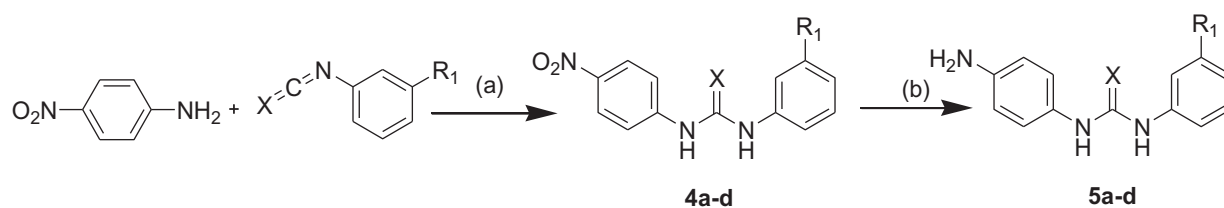


Figure 3. Examples of dual inhibitors acting on EGFR and VEGFR2.



Scheme 1. Synthesis of ethyl (4-chloro-5-methylthieno[2,3-*d*]pyrimidine)-6-carboxylate. Reagents and conditions: (a) Morpholine, S, EtOH, 70 °C, 4 h, 0 °C, 24 h; (b) Formamide, acetic acid, 40 h., 150 °C; (c) POCl₃, reflux, 3 h.



Code	5a	5b	5c	5d
X	O	O	O	S
R ₁	H	OCH ₃	CF ₃	H

Scheme 2. Synthesis of 1-(4-aminophenyl)-3-phenylurea and 1-(4-aminophenyl)-3-phenylthiourea derivatives. Reagents and conditions: (a) DCM, rt, 24 h. (b) H₂, Pd/C, MeOH, rt, 4 h.

hydroxylamine in absolute ethanol to give (**15a-d**)^{26,27}, (Scheme 4). Then, the hydrolysis of the carboxylate ethyl ester of the previously prepared compounds (**14b-d**) (Scheme 4), through refluxing it with Li(OH)₂ in THF and water to prepare the intermediate carboxylic acid derivatives (**16b-d**)²⁸. The previously prepared carboxylic acid derivatives (**16b-d**) are coupled with the appropriate amino acid ester hydrochloride salt, utilising EDCI with HOBt in dry DMF²⁹, to obtain a high yield of novel intermediate compounds (**17b-d and 18b-d**), (Scheme 4). Finally, the ethyl ester group in the previously prepared novel compounds (**17b-d, 18b-d**) reacted with freshly prepared hydroxylamine in absolute ethanol to obtain target novel hydroxamic acid derivatives (**19b-d, 20b-d**) confirmed by many spectral data, (Scheme 4).

3.2. Biological evaluation

The target compounds were evaluated for their *in vitro* inhibitory activities against EGFR, VEGFR-2, and HDAC6. The EGFR and VEGFR-2 inhibitory assays were performed at Thermo Fischer Scientific, Madison, WI, USA (SelectScreenServices@thermofisher.com). The HDAC inhibitory assays were performed at BPS Bioscience, San Diego, CA, USA (www.bpsbioscience.com). Initially, all of the synthesised target compounds were evaluated for their percent inhibitory activity against EGFR, VEGFR-2, and HDACs at 10 μM single dose concentration, in which their mean percent inhibition is summarised in (Figure 5, Tables 1 and 2). Representative compounds were evaluated for their percent inhibitory activity against EGFR and VEGFR-2 at 6 different concentrations (0.1 nM, 1 nM, 10 nM, 100 nM, 1 μM, 10 μM) to subsequently calculate their IC₅₀ values (Table 3). Additionally, all of the synthesised target compounds were submitted to the National Cancer Institute "NCI" Bethesda, Maryland, USA (www.dtp.nci.nih.gov), to evaluate their *in vitro* antiproliferative activities against NCI 60- cancer cell line panel.

3.2.1. In vitro EGFR inhibitory assay

By closely investigating the structure activity relationship, thieno[2,3-d]pyrimidine derivatives with aniline moiety showed an excellent inhibitory profile compared to derivatives with urea and benzimidazole moieties (Tables 1 and 2). Moreover, thieno[2,3-d]pyrimidine derivatives with aniline moiety, mono-substitutions, or di-substitutions at 3- or 4- positions on its terminal phenyl ring exhibited excellent inhibitory profile, as previously reported³⁰.

In general, EGFR inhibition increases by increasing the number of carbons in the linker chain between the hydroxamic acid moiety and the amide group to three carbons or by directly attaching the hydroxamic acid with the thienopyrimidine fragment. So that compounds (**20b and 20c**) showed 92 and 96% inhibition, compared to inhibition of 76 and 78% for the two carbons linker of (**19b and 19c**), respectively (Table 2).

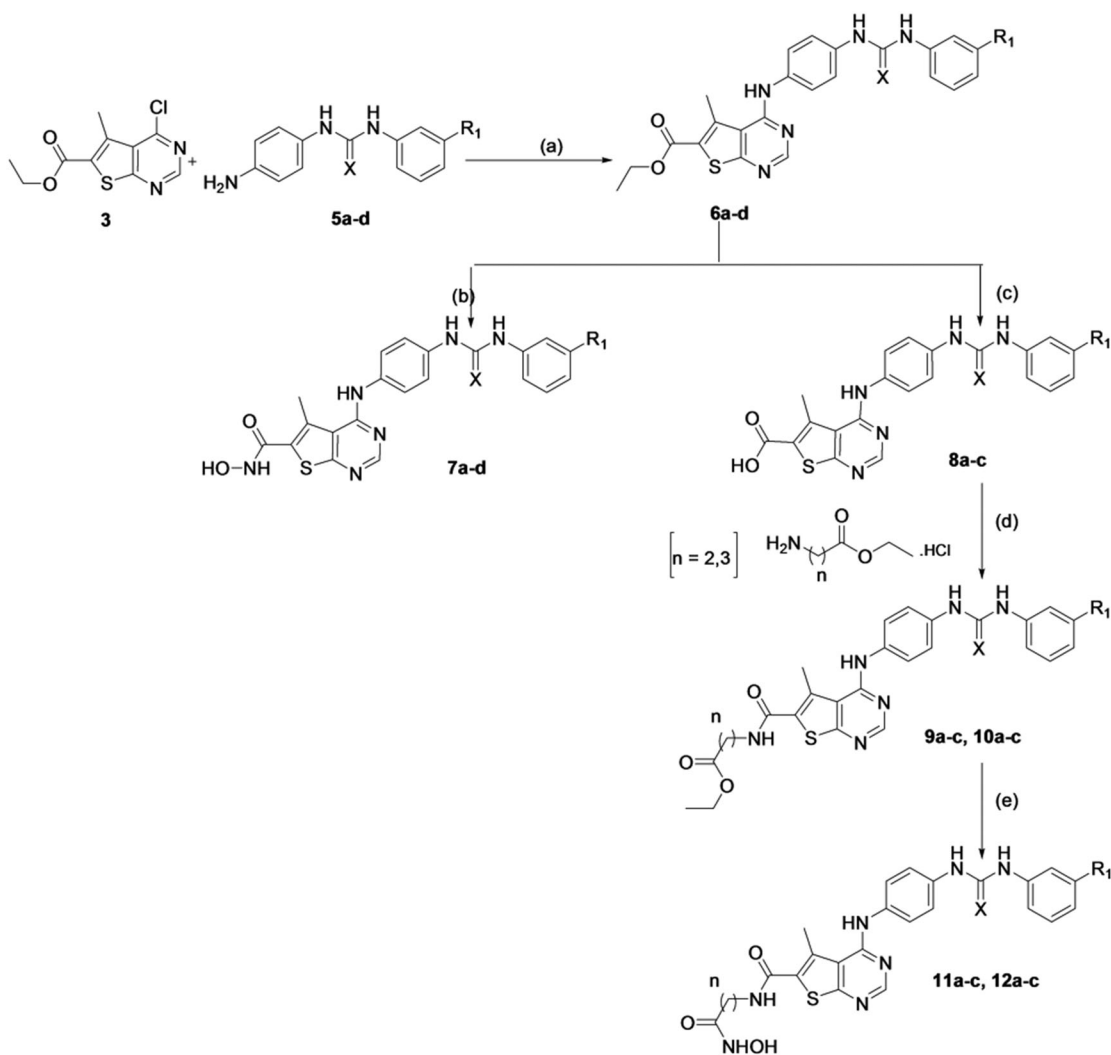
Remarkably, compound (**12c**) bearing urea moiety with 3-CF₃ at its terminal phenyl ring showed an exceptional significant inhibitory activity towards EGFR kinase activity (66%), compared to other thieno[2,3-d]pyrimidine derivatives bearing urea moiety. Also, compound (**7d**) bearing thiourea demonstrated noticeable higher inhibitory activity (78% inhibition) than compound (**7a**) bearing urea moiety (48% inhibition).

Promising candidates, (**12c, 15c, 20b and 20d**) were chosen as representatives for evaluation of potential enzyme inhibitory activity (IC₅₀) (Table 3). Compound (**15c**) demonstrated the most potent EGFR inhibition with IC₅₀ value of 19 nM since its hydroxyl amine group is directly attached to the thieno[2,3-d]pyrimidine ring and also it has 4-Cl substitution on its terminal phenyl ring. Compound (**20d**) exhibited more potent inhibition than (**20b**) with IC₅₀ value of 68 nM compared to 155 nM. Since both (**20d and 20b**) have a linker of 3 carbons, thus the (4-F, 3-Cl) substitution at the terminal phenyl ring of compound (**20d**) is suggested to be responsible for the increase of its inhibitory activity compared to (**20b**), with no substitution at its terminal phenyl ring.

Noticeably, compound (**12c**) bearing urea moiety with 3-CF₃ at its terminal phenyl ring exhibited IC₅₀ value of 1.14 μM, in which it showed the highest EGFR inhibition among all other synthesised derivatives bearing urea moiety.

3.2.2. In vitro VEGFR-2 inhibitory assay

On the contrary of EGFR inhibitory assay, most of the thieno[2,3-d]pyrimidine derivatives bearing urea moiety (**7a-c, 11b,c, 12b,c**) have demonstrated potent inhibition ranging from (75-100%) for VEGFR-2 kinase activity at an initial screening of 10 μM concentration. Compounds with 3-CF₃ substitution at its terminal phenyl ring (**7c, 11c and 12c**) demonstrated the most potent VEGFR-2 inhibition by 100, 91 and 100%, respectively (Table 1). Moreover, by observing the effect of the hydrocarbon linker on the VEGFR-2 inhibitory activity, it was found that the most potent inhibitory activities were observed with derivatives bearing urea moieties having hydroxylamine moiety directly attached to the thieno[2,3-d]pyrimidine ring, such as (**7a, 7b and 7c**) exhibited 89, 78 and



Code	7a	7b	7c	7d	11a			12a		
					n = 2			n = 3		
X	O	O	O	S	O	O	O	O	O	O
R ₁	H	OCH ₃	CF ₃	H	H	OCH ₃	CF ₃	H	OCH ₃	CF ₃

Scheme 3. Synthesis of phenyl ureido phenyl amino thieno [2,3-d] pyrimidine hydroxamic acid derivatives. Reagents and conditions: (a) EtOH, TEA, reflux, 18–48 h; (b) NH₂OH.HCl, MeOH, Na, 0 °C; (c) Li(OH)₂, THF, reflux, 7 h; (d) EDCI/HOBt, NMM, DMF, 0 °C, rt, 24 h; (e) NH₂OH.HCl, EtOH/Na, 0 °C.

100% inhibition, respectively. Noticeably, compound (**7a**) bearing a urea moiety showed higher VEGFR-2 inhibition (89% inhibition) than compound (**7d**) bearing thiourea moiety (45% inhibition) (Table 1).

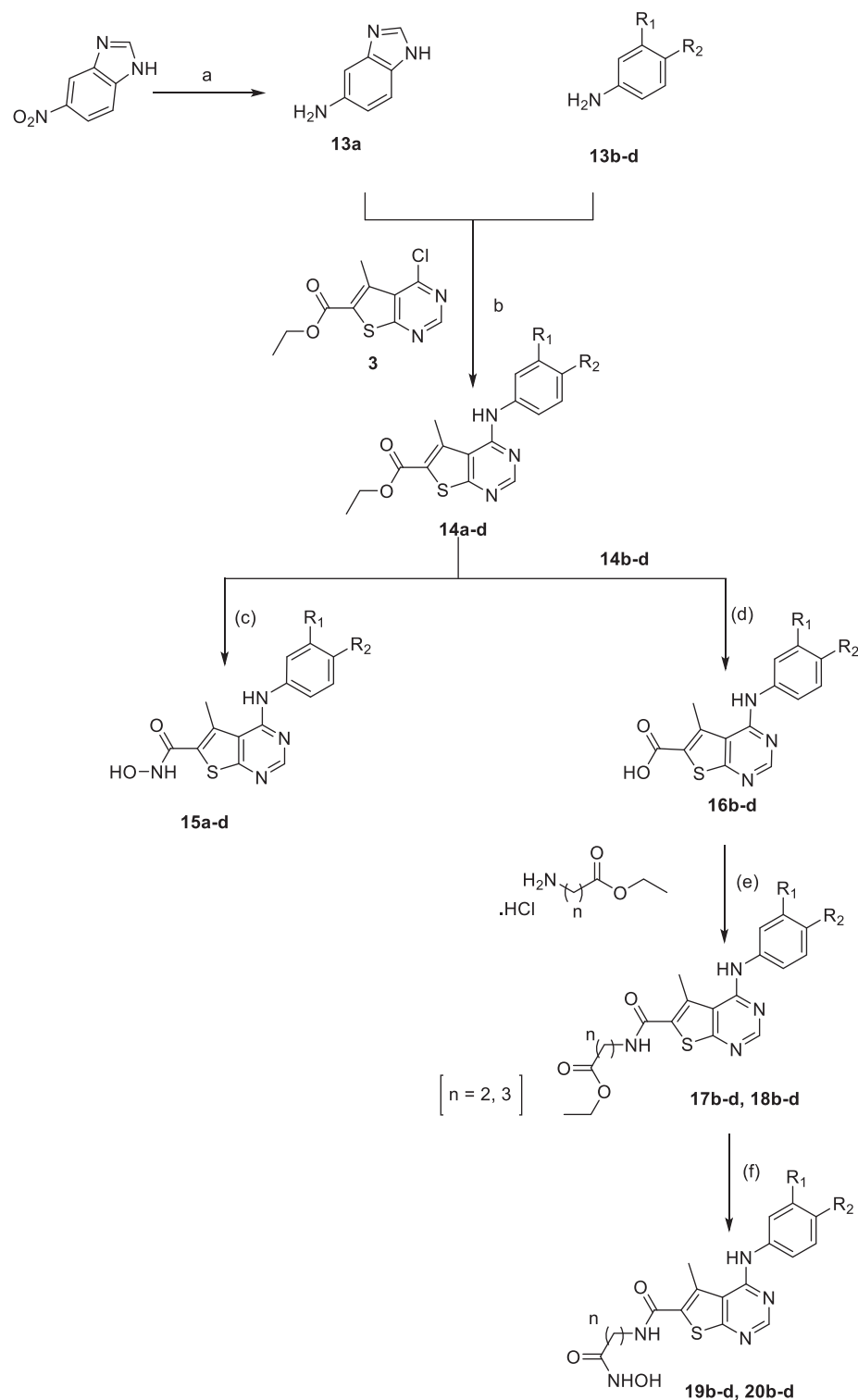
As for the aniline series, compound (**17c**) with no linear hydrocarbon linker between the hydroxamic acid moiety and the thieno[2,3-d]pyrimidine fragment and 4-chloro substitution on its terminal phenyl ring showed exceptional potent inhibition (87% inhibition) (Table 2).

Promising candidates, (**7c**, **12c**, and **15c**) were chosen as representatives for the evaluation of potential enzyme inhibitory activity (IC₅₀) (Table 3). All of the evaluated target compounds exhibited potent VEGFR-2 inhibitory activity with IC₅₀ values ranging from (185 nM to 5.58 μM). Compounds (**7c** and **12c**) bearing urea moiety exhibited potent VEGFR-2 inhibition with IC₅₀ values of 191 and 185 nM, respectively. These results suggest that -CF₃ substitution at the terminal phenyl ring of compounds (**7c** and **12c**) and the urea moiety is responsible for their high inhibitory

activity, regardless of having 3 carbons in the linker chain (**12c**) or without having a linker (**7c**). Compound (**15c**) with 4-chloro aniline moiety exhibited significant inhibition to VEGFR-2 with a higher IC₅₀ value of 5.58 μM than other derivatives bearing urea moiety.

3.2.3. In vitro HDAC inhibitory assay

Initially, all synthesised compounds were screened against HDAC6 at 10 μM concentration. HDAC6 enzyme inhibition assay was selected since our newly synthesised hydroxamic acid compounds have a large capping group suitable for fitting in the large hydrophobic channel of HDAC6, which is unique to the HDAC6 receptor²⁶. The newly designed compounds were synthesized either having short hydrocarbon linkers between the zinc-binding group (ZBG) and the connecting amide unit or having no linear hydrocarbon linker between the hydroxamic acid moiety and the



Code	15b	15c	15d	19b	19c	19d	20b	20c	20d
				n=2			n=3		
R₁	H	H	Cl	H	H	Cl	H	H	Cl
R₂	H	Cl	F	H	Cl	F	H	Cl	F

Scheme 4. Synthesis of 5-amino benzimidazole thieno [2,3-d] pyrimidine hydroxamic acid derivative and 4-anilino thieno [2,3-d] pyrimidine hydroxamic acid derivatives. Reagents and conditions: (a) H₂, Pd/C, MeOH, rt, 6 h; (b) EtOH, TEA, reflux, 18–48 h; (c) NH₂OH.HCl, MeOH/Na, 0 °C; (d) Li(OH)₂, THF, reflux, 7 h; (e) EDCI/HOBt, NMM, DMF, 0 °C, rt, 24 h; (f) NH₂OH.HCl, EtOH/Na, 0 °C.

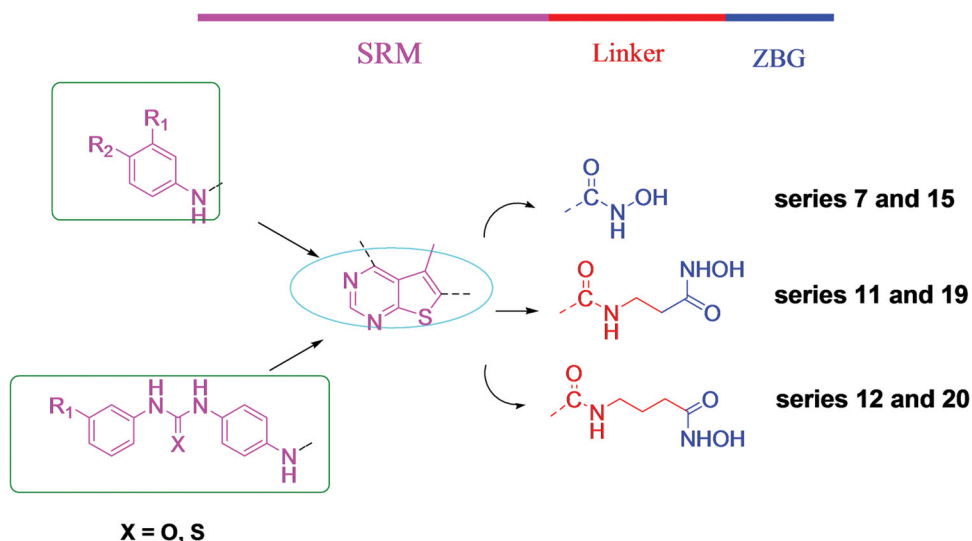


Figure 4. Design strategy of hybrid multitarget (EGFR, VEGFR, and HDAC inhibitors). Colour codes show essential pharmacophore for HDAC inhibitors composed of surface recognition moiety (purple), linker (red), and zinc-binding group (blue). The cyan oval shape represents the area binding to the hinge region of the ATP binding site of VEGFR2 and EGFR and the green square represents the area binding to the hydrophobic pocket of VEGFR2 and EGFR, while the rest of the structure represents the area fitting in the solvent-accessible area of VEGFR2 and EGFR.

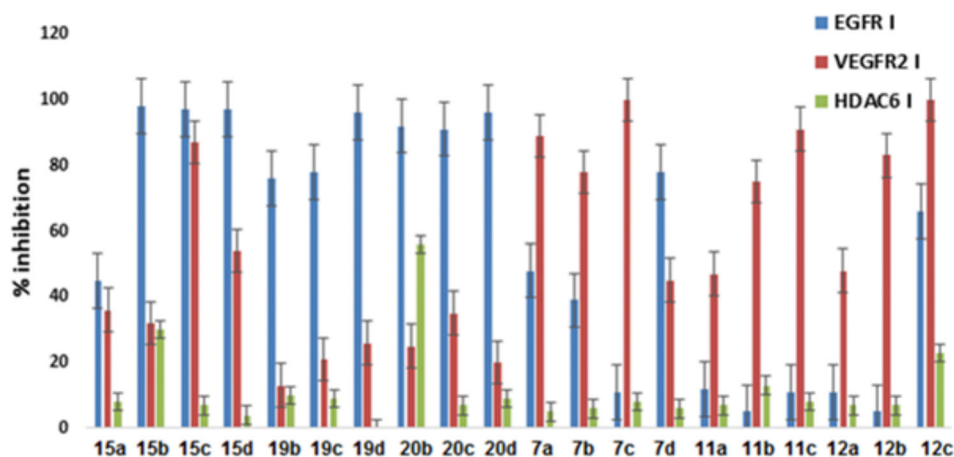


Figure 5. Mean % inhibition of the investigated compounds on EGFR, VEGFR-2 and HDAC6 at 10 μM concentration.

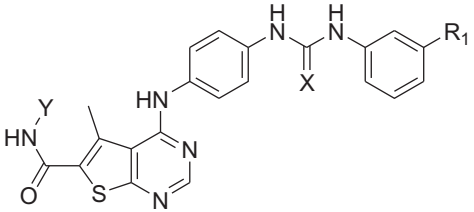
thieno[2,3-*d*]pyrimidine fragment, as the previously reported potent HDAC6 inhibitors^{19,20}.

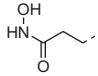
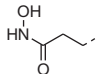
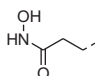
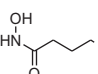
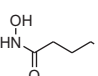
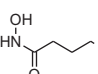
Screening of the synthesised compounds against HDAC6 at 10 μM concentration is shown in (Tables 1 and 2). For derivatives bearing urea moiety, compound (**12c**) with three carbons in the linker region showed considerable HDAC6 inhibition by 23% (Table 1). For derivatives bearing aniline moiety, compound (**20b**) exhibited the most significant HDAC6 inhibition by 56% (Table 2). Compound (**20b**); bearing unsubstituted aniline moiety; is the smallest capping group among all synthesised compounds. The small capping group may allow it to fit in the HDAC6 hydrophobic channel. Additionally, compound (**20b**) had 3 carbons in the linker region compared to (**15b**) with no linear hydrocarbon linker and (**19b**) with 2 carbons in the linker region showing 30% and 10% inhibition, respectively (Table 2). Thus, having a small capping group of unsubstituted aniline and a longer carbon chain in the

linker region between the hydroxamic acid moiety and the connecting amide is recommended for optimum HDAC6 inhibition.

In conclusion, potential novel multitarget hybrid lead inhibitors acting on EGFR, VEGFR-2 and HDAC6 are considered, such as compounds (**12c**, **15b** and **20b**). Compound (**12c**) exhibited potent VEGFR-2 inhibition (100%, $\text{IC}_{50} = 185 \text{ nM}$), significant EGFR inhibition (66%, $\text{IC}_{50} = 1.14 \mu\text{M}$) and mild HDAC6 inhibition (23%). Compound (**15b**) exhibited potent EGFR inhibition (98%), moderate VEGFR-2 (32%) and moderate HDAC6 inhibition (30%). Compound (**20b**) exhibited potent EGFR inhibition (92%, $\text{IC}_{50} = 155 \text{ nM}$), moderate HDAC6 inhibition (56%) and mild VEGFR-2 inhibition (25%), (Figure 5).

Moreover, many of the synthesised novel compounds can be considered as promising leads of EGFR and VEGFR-2 dual inhibitors, (Table 2 and Figure 5). Where, compound (**15c**) is considered to be the most potent dual inhibitor among all the synthesised

Table 1. Mean % inhibition of the investigated compounds on EGFR, VEGFR-2 and HDAC6 at 10 μ M concentration.


Code	R1	X	Y	EGFR	VEGFR-2	HDAC6
7a	H	O	OH	48%	89%	5%
7b	OCH ₃	O	OH	39%	78%	6%
7c	CF ₃	O	OH	11%	100%	8%
7d	H	S	OH	78%	45%	6%
11a	H	O		12%	47%	7%
11b	OCH ₃	O		5%	75%	13%
11c	CF ₃	O		11%	91%	8%
12a	H	O		11%	48%	7%
12b	OCH ₃	O		5%	83%	7%
12c	CF ₃	O		66%	100%	23%

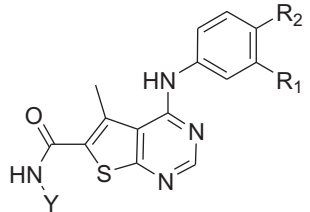
Red-coloured data represent potent inhibition 70–100%, green-coloured data represent moderate inhibition 30–70%, blue-coloured data represent mild inhibition 20–30%, and the black-coloured data represent very weak inhibition <20%.

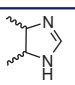
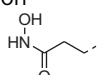
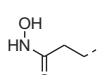
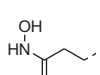
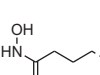
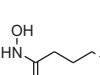
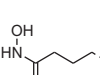
compounds, since it exhibits potent EGFR and VEGFR-2 inhibition (97%, IC_{50} = 19 nM) and (87%, IC_{50} = 5.58 μ M), respectively. Compound (**15d**) exhibited potent EGFR and moderate VEGFR-2 inhibition (97%) and (54%), respectively. Two selective potent inhibitors were also considered, such as (**7c** and **20d**). Compound (**7c**) is considered as a potent novel VEGFR-2 inhibitor (100% inhibition, IC_{50} = 191 nM), while compound (**20d**) is considered as a potent novel EGFR inhibitor (96% inhibition, IC_{50} = 68 nM).

3.2.4. In vitro antiproliferative activity

All of the synthesised structures were selected and submitted to NCI based on computer modelling techniques and the degree of diversity of structures for the evaluation of their antiproliferative activity. The 20 synthesised compounds were selected with their respective NCI codes [NCS D-820157- NCS D-820176] for the inhibition percent assay at an initial single dose of 10 μ M on the full NCI 60 cell panel, where the mean graph of the percent growth for all compounds on the full NCI cell panel is evaluated, compared to the untreated control cells (Supplementary Material). *In vitro* cell line inhibition % of all synthesised compounds is represented in (Table 1 of Supplementary Material).

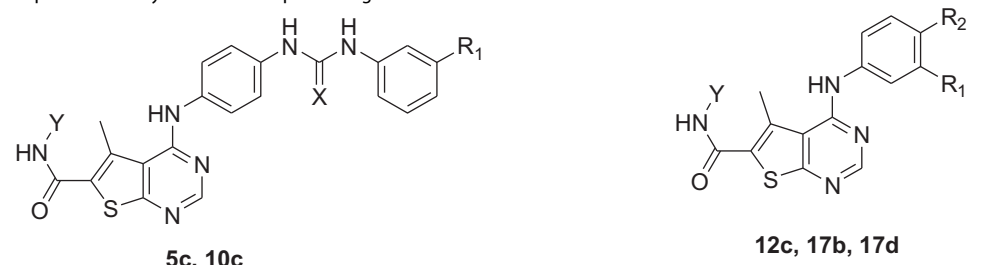
First, in series (**7a-d**) bearing urea moiety with no linear hydrocarbon linker between the hydroxamic acid moiety and the

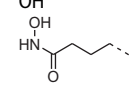
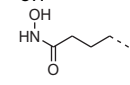
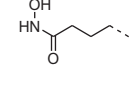
Table 2. Mean % inhibition of the investigated compounds on EGFR, VEGFR-2, and HDAC6 at 10 μ M concentration.


Code	R1	R2	Y	EGFR	VEGFR-2	HDAC6
15a			OH	45%	36%	8%
15b	H	H	OH	98%	32%	30%
15c	H	Cl	OH	97%	87%	7%
15d	Cl	F	OH	97%	54%	4%
19b	H	H		76%	13%	10%
19c	H	Cl		78%	21%	9%
19d	Cl	F		96%	26%	0%
20b	H	H		92%	25%	56%
20c	H	Cl		91%	35%	7%
20d	Cl	F		96%	20%	9%

Red-coloured data represent potent inhibition 70–100%, green-coloured data represent moderate inhibition 30–70%, blue-coloured data represent mild inhibition 20–30%, and the black-coloured data represent very weak inhibition <20%.

thieno[2,3-*d*]pyrimidine fragment, compound (**7c**) with urea moiety and 3-CF₃ at the terminal phenyl ring showed the most significant anti-proliferative activity among all of the synthesised compounds, where it exhibited inhibitory activity against the central nervous system (CNS) cancer [SNB-75 cancer cell line (46% inhibition) and SF-539 cancer cell line (38.6% inhibition)] and colon cancer KM12 cancer cell line (33.7% inhibition). (**7c**) exhibited inhibition activity also against CNS cancer [U251 cancer cell line (26.9% inhibition) and SF-268 cancer cell line (10.8% inhibition)], renal cancer UO-31 (24.7% inhibition), leukaemia MOLT-4 (11.8% inhibition), NSCLC [NCI-H522 cancer cell line (11.7% inhibition) and NCI-H23 (11.1% inhibition)] and breast cancer MCF7 cancer cell line (11.6% inhibition). While in series (**15a-d**) bearing aniline moiety with no linear hydrocarbon linker between hydroxamic acid moiety and thieno[2,3-*d*]pyrimidine fragment, compound (**15c**) with 4-Cl aniline exhibited inhibitory activity mostly against renal cancer UO-31 cancer cell line (28.8% inhibition), NSCLC [NCI-H522 cancer cell line (25.4% inhibition) and

Table 3. The IC₅₀ value of representative synthesised compounds against EGFR and VEGFR-2.


Code	Compound				IC ₅₀ in enzyme assays	
	R1	R2	X	Y	EGFR	VEGFR-2
7c	CF ₃	-	O	OH	ND	191 nM
12c	CF ₃	-	O		1.14 μM	185 nM
15c	H	Cl	-	OH	19 nM	5.58 μM
20b	H	H	-		155 nM	ND
20d	Cl	F	-		68 nM	ND
Gefitinib [27]					1.08 μM	ND
Vandetanib [17]					0.5 μM	40 nM

ND: not determined.

EKVX cancer cell line (20.6% inhibition)] and CNS cancer SNB-75 cell line (20.4% inhibition).

In series (**12a-c**) bearing urea moiety with three carbons in the linker chain between the hydroxamic acid moiety and the amide group, compound (**12c**) with urea moiety and CF₃ at the terminal phenyl ring showed moderate inhibitory activity mostly against CNS cancer [SNB-75 cancer cell line (29.2% inhibition) and SF-539 cell line (28.5% inhibition)]. In series (**20b-d**) bearing aniline moiety with three carbons in linker chain between the hydroxamic acid moiety and the amide group, compound (**20d**) exhibited inhibitory activity mostly against renal cancer UO-31 cancer cell line (23.7% inhibition), breast cancer MDA-MB-468 (16.2% inhibition) and NSCLC NCI-H226 (11.3% inhibition).

In series (**11a-c**) and (**19b-d**) with two carbons in the linker chain between the hydroxamic acid moiety and the amide group, most of the compounds showed lower inhibitory activities against most of the investigated cell lines.

Recent studies revealed that VEGFR-2 is a major contributor to the growth of CNS tumours and its interruption may effectively suppress tumour growth in CNS cancer³¹. It was also reported that VEGFR-2 is a promising platform for anti-angiogenesis cancer therapy for colon cancer cells³². Also, EGFR was reported to be overexpressed in different cancer cell lines, including NSCLC³³, renal cancer³⁴, and brain cancer³⁵. Noticeably, it is observed that most of the compounds showed weak to moderate inhibition towards Renal UO-31 and CNS cancer SNB-75 cell lines (20–46% inhibition).

From these findings, it is suggested that the potent *in vitro* inhibition of compound (**7c**) towards VEGFR-2 (100% inhibition, IC₅₀ = 191 nM) contributed to the significant inhibitory activity against CNS [SNB-75 cancer cell line (46% inhibition) and SF-539 cancer cell line (38.6% inhibition)] and colon KM12 cancer cell line (33.7% inhibition). It is also suggested that the potent *in vitro* inhibition of compound (**15c**) towards EGFR (97% inhibition, IC₅₀

= 19 nM) and VEGFR2 (87% inhibition, IC₅₀ = 5.58 μM) contributed to the significant inhibitory activity against renal, CNS and NSCLC cancer cell lines as discussed. Additionally, it is also observed that (**15c**) is the only compound that showed considerable inhibition towards NSCLC H522 (25.4% inhibition) and EKVX (20.6% inhibition) cancer cell lines, which is contributed to its potent EGFR inhibition with (IC₅₀ = 19 nM).

It is obvious that despite most of our newly synthesised compounds exhibited potent EGFR and/or VEGFR-2 *in vitro* inhibitory activities (90–100% inhibition) but unexpectedly some of the compounds showed moderate *in vitro* inhibitory activity against NCI cell lines at 10 μM concentration. It is suggested that maybe the increased polarity of our synthesised hydroxamic acids, might contribute to poor cell membrane permeability towards NCI cancer cell lines. Also, VEGFR-2 inhibitors showed less sensitivity towards NCI cancer cell lines than human vascular endothelial cells, which contributed to their moderate antiproliferative activity towards NCI cancer cell lines³⁰.

3.3. Molecular modelling studies

3.3.1. Docking study

A molecular docking study using Discovery Studio 4.5 was performed using the C-DOCKER algorithm. A docking study is performed to analyse binding affinities, binding modes, and orientation of the newly synthesised target compounds into the active binding site of three different receptors such as EGFR, VEGFR-2, and HDAC6. The best docking pose is selected based on its binding mode in comparison to that of the reference ligand. The crystal structure of EGFR, VEGFR-2, and HDAC6 co-crystallised with their reference ligands were downloaded from protein data bank (www.rcsb.org) with PDB codes: 4HJO, 3VHE, and 5G0H, respectively. Re-docking the reference compounds into the X-ray

crystal structure of the active site of its receptor was performed for validation.

3.3.1.1. Docking study on EGFR. The first docking study was done on EGFR (PDB code 4HJO) co-crystallised with the reference ligand (erlotinib). The root mean square difference (RMSD) between the re-docked and the co-crystallised conformers of erlotinib is 0.5 Å, which signifies the validity of the C-DOCKER algorithm. Besides, re-docked erlotinib retrieved the reported binding mode into the active binding site of EGFR (-CDOCKER energy = 27.18 Kcal/mol) as depicted in (Figure 6)³⁶. Where nitrogen of pyrimidine ring forms a hydrogen bond with NH of MET769, pyrimidine ring forms hydrophobic interactions with ALA719, MET769 and LEU820, phenyl ring forms hydrophobic interaction with LEU694 and LEU820 and the terminal phenyl ring forms hydrophobic interaction with VAL702, ALA719 and LYS721 (Figure 6). Docking of all synthesised compounds was done on EGFR (PDB code 4HJO), where the binding mode of representative thieno[2,3-*d*]pyrimidine derivatives were investigated to justify the potent or significant EGFR inhibition (high % inhibition or low IC₅₀) exhibited by some of the synthesised compounds (Table 2 of Supplementary Material). In general, docking results revealed that thieno[2,3-*d*]pyrimidine derivatives with aniline moiety (**15c**, **15d**, **19d**, **20b-d**) showed higher binding affinities than erlotinib, fulfilled the reported binding mode and showed extra interactions with EGFR active site. Although thieno[2,3-*d*]pyrimidine derivatives with urea moiety showed higher binding affinities than erlotinib but it did not fulfil all the key interactions with the active site of EGFR. The binding mode and energies of three representatives docked compounds are presented in (Figure 7). Compound (**15c**) showed the most potent EGFR inhibitory activity (97%, IC₅₀ = 19 nM) and revealed better binding affinity than erlotinib (-CDOCKER energy = 28.34 Kcal/mol). The binding mode of (**15c**) was consistent with erlotinib as shown in (Table 2 of Supplementary Material). Additionally, the methyl group of (**15c**) showed extra hydrophobic interactions with VAL702 and LEU820 and chlorine showed extra hydrophobic interactions with adjacent hydrophobic pockets including LEU764 and LEU834. Compound (**20d**) exhibited potent inhibitory activity towards EGFR (97%, IC₅₀ = 68 nM) and revealed better binding affinity than erlotinib (-CDOCKER energy = 42.52 Kcal/mol). The binding mode was consistent with erlotinib as shown in (Table 2 of Supplementary Material), where the oxygen of the hydroxyl group showed 2 additional hydrogen bonds with LYS692 and VAL693, oxygen of hydroxamic carbonyl group and hydrogen of hydroxamic amine showed extra hydrogen bonds with LYS692 and LEU694, respectively. Moreover, the methyl group of (**20d**) showed additional hydrophobic interaction with VAL702, and chlorine showed additional hydrophobic interaction with ALA719 and LYS721. Compound (**12c**) bearing urea moiety exhibited significant EGFR inhibitory activity (66%, IC₅₀ = 1.14 μM), but it showed lower inhibition than other compounds bearing aniline moiety. Compound (**12c**) revealed a missing hydrogen bond with the essential MET796 although having better binding affinity than erlotinib (-CDOCKER energy = 43.31 Kcal/mol). Compound (**12c**) showed five extra hydrogen bonds, where the oxygen of carbonyl urea showed hydrogen bond with THR766, oxygen of hydroxamic carbonyl group showed hydrogen bond with CYS773, oxygen of hydroxyl group showed hydrogen bond with PHE771, F of terminal phenyl ring showed hydrogen bond with PHE832 and hydrogen of urea amine showed hydrogen bond with ASP831. Additionally, the three fluorine atoms of CF₃ showed three halogen interactions with CYS751 and one halogen interaction with ARG752. Pyrimidine ring of (**12c**) forms

hydrophobic interactions with LEU694 and LEU820, thiophene ring forms hydrophobic interaction with LEU694, phenyl ring forms hydrophobic interaction with VAL702 and LEU820 and terminal phenyl ring shows four hydrophobic interactions with extra hydrophobic pocket including LEU753, LEU764, LEU834, and MET742. Moreover, a methyl group and C of CF₃ of (**12c**) showed additional hydrophobic interactions with LEU694 and CYS751, respectively.

3.3.1.2. Docking study on VEGFR-2. The second docking study was done on VEGFR-2 (PDB code: 3VHE) co-crystallised with the reference compound; (pyrrolo[3,2-*d*]pyrimidine derivative;). RMSD between the re-docked and the co-crystallised conformer of the reference is 0.5 Å, which proves the validity of the C-DOCKER algorithm. Noticeably, redocked pyrrolo[3,2-*d*]pyrimidine reference compound (-C-DOCKER energy = 42.91 Kcal/mol) retrieved the reported binding mode into the active site of VEGFR-2 (pdb code: 3VHE)³⁰ as depicted in (Figure 8). Where nitrogen of pyrimidine ring showed hydrogen bond with CYS919 in the ATP-binding site (hinge region), the oxygen of urea carbonyl group formed hydrogen bond with ASP1046, while the two NH of urea moiety showed bifurcate hydrogen bonds with GLU885. Additionally, the pyrrole ring showed hydrophobic interactions with CYS919, LEU840, ALA866, VAL848 and LEU1035, the pyrimidine ring formed hydrophobic interactions with CYS919, ALA868, VAL848 and LEU1035. Furthermore, the phenyl ring showed hydrophobic interactions with VAL848, VAL899, LYS868, CYS1045 and pi-pi interaction with PHE1047. Finally, the terminal phenyl ring formed hydrophobic interaction with LEU889. Docking of all synthesised derivatives was done on VEGFR-2 (PDB code: 3VHE), where the binding mode of representative thieno[2,3-*d*]pyrimidine derivatives was explored to justify the potent or significant VEGFR-2 inhibition exhibited by some of the synthesised compounds (Table 3 of Supplementary Material).

In general, docking results revealed that most of the thieno[2,3-*d*]pyrimidine derivatives with urea moiety (**7c** and **12c**) showed higher binding affinities than the reference compound and compounds with aniline moiety (**15c**) which is consistent with VEGFR-2 inhibition assay. In which, compounds bearing urea moiety, such as (**12c**) with (IC₅₀ = 185 nM), and (**7c**) with (IC₅₀ = 191 nM) exhibited potent VEGFR-2 inhibition compared to compound (**15c**) bearing aniline moiety with (IC₅₀ = 5.58 μM). Where (**12c**) and (**7c**) retrieved all the essential hydrogen bond and hydrophobic interactions of the reference compound, while compound (**15c**) missed the essential hydrogen bond interactions with GLU885 and ASP1046 although its pyrimidine ring retrieved the essential hydrogen bond with CYS919 (Table 3 of Supplementary Material). The binding interactions and energies of two representatives docked compounds are presented in (Figure 9). Additionally, we found that compounds (**12c**) and (**7c**); both bearing urea moiety with CF₃ substituent and compound (**15c**) bearing 4-chloro aniline moiety showed higher binding affinities and made extra hydrophobic bonds than the reference compound. Where CF₃ in compound (**12c**) made extra hydrophobic bonding with ILE892, LEU1019 and HIS1026, F of CF₃ in compound (**7c**) made an extra halogen hydrogen bond with HIS1026 and 4-Cl of the terminal phenyl ring in compound (**15c**) forms additional hydrophobic interaction with LEU889, VAL899 and LYS868. According to previously reported SAR, this area is an allosteric hydrophobic binding pocket revealed for type II VEGFR inhibitors, in which the phenylalanine residue of the DFG loop flips out of its lipophilic pocket to increase the binding affinity of inhibitors to VEGFR receptors and increase residence time^{37,38}.

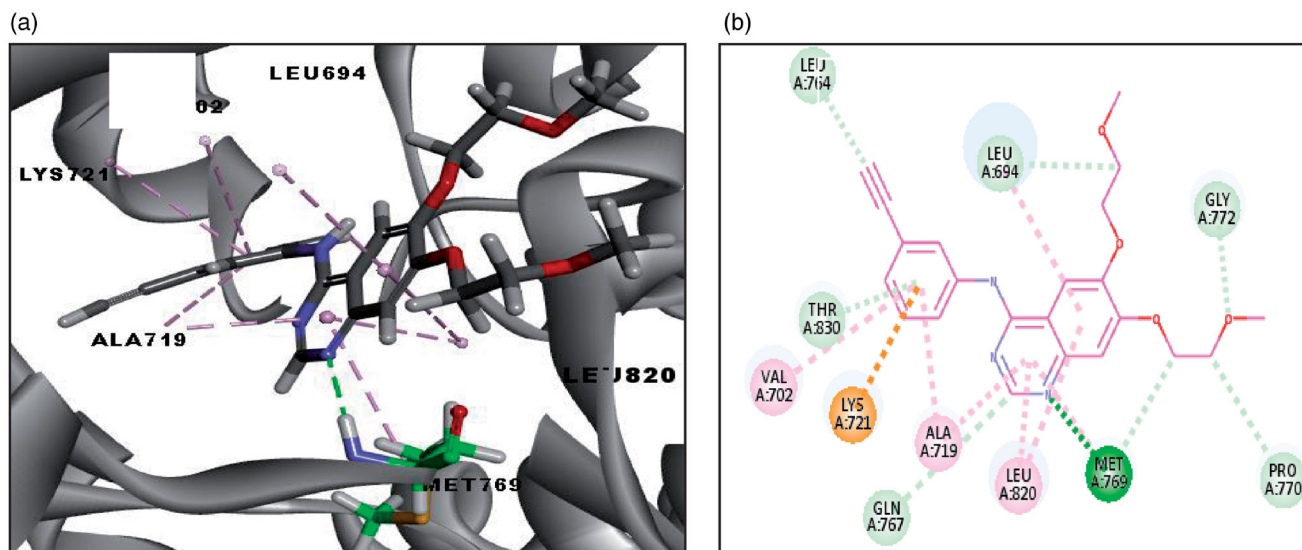


Figure 6. (a) 3D image of binding interaction of Erlotinib (-CDOCKER energy = 27.18) with EGFR (with PDB code: 4HJO) using Accelrys Discovery Studio 4.5. (b) 2D image of binding interaction of Erlotinib with EGFR. Hydrogen bond interaction is described as green dotted line, hydrophobic interactions are described as purple-dotted lines and electrostatic interactions are described as orange-dotted lines.

3.3.1.3. Docking study on HDAC6. The final docking study was done on HDAC6 (PDB code: 5G0H) co-crystallised with the reference compound (Trichostatin A; TSA). RMSD is 0.44 Å, which signifies the validity of CDOCKER algorithm. Moreover, the reported binding mode³⁹ of TSA was retrieved into the X-ray crystal structure of HDAC6 (-CDOCKER energy = 25.49) as shown in (Figure 10), where the oxygen of hydroxamic hydroxyl group forms a hydrogen bond with HIS573 and oxygen of both hydroxamic carbonyl and hydroxyl groups forms coordinate bonds with zinc metal in a bidentate fashion with distances 2.24 Å and 2.20 Å, respectively. Additionally, the phenyl ring of TSA shows pi-pi stacking with PHE643 and the aliphatic chain of the linker showed hydrophobic interaction with PHE583 and PHE643 (Figure 10). Docking of all synthesised compounds was performed on HDAC6 (PDB code: 5G0H), where the binding mode of representative thieno[2,3-*d*]pyrimidine derivatives were explored to justify the significant inhibition of compound (**20 b**) (56% inhibition) against HDAC6 among other derivatives that showed remarkably lower % inhibition against HDAC6 (Table 4 of Supplementary Material).

The binding interactions and energies of three representatives docked compounds (**12c**, **19 b** and **20 b**) are presented in (Figure 11). Compound (**20 b**) with unsubstituted aniline moiety and three carbons in the linker region exhibited the most significant HDAC6 inhibition among all the synthesised compounds (56% inhibition) and it revealed higher binding affinity than TSA (-CDOCKER energy = 34.32). This significant inhibitory activity for (**20 b**) was justified by its consistent binding mode with the reported binding mode of TSA against HDAC6 (PDB: 5G0H), where the oxygen of hydroxamic carbonyl and hydroxyl groups forms coordinate bonds with zinc metal in a bidentate fashion with distances 2.24 Å and 2.36 Å, respectively. The oxygen of the hydroxamic hydroxyl group forms a hydrogen bond with HIS573 and oxygen of hydroxamic and amidic carbonyl group forms two additional hydrogen bonds with TYR745 and HIS614, respectively. Also, the thiophene ring of (**20 b**) shows pi-pi stacking with PHE643. While, compound (**19 b**) with unsubstituted aniline moiety and two carbons in the linker region exhibited insignificant inhibitory activity (10%), although it revealed higher binding affinity (-CDOCKER energy = 37.68) than (**20 b**) (Figure 11). By comparing the binding mode of compounds (**20 b**) and (**19 b**), it was found that the insignificant inhibitory

activity of the compound (**19 b**) is certainly accounted for by having a shorter linker between the hydroxamate moiety and the connecting amide group (two carbons) than compound (**20 b**) (3 carbons) since they both bear the same hydrophobic cap group. The shorter two carbons linker of compound (**19 b**) contributes to its failure to form a coordinate bond with zinc metal in a bidentate fashion, where the oxygen of hydroxamic carbonyl group forms only one coordinate bond with zinc metal (Figure 11). Whereas compound (**12c**) with urea moiety exhibited lower HDAC6 inhibition (23%) than (**20 b**), although it revealed higher binding affinity (-CDOCKER energy = 37.58) than (**20 b**) and TSA. The decrease in HDAC6 inhibition by compound (**12c**) is justified by its binding mode as described in (Figure 11), in which the oxygen of hydroxamic carbonyl group forms only one coordinate bond with zinc metal in a monodentate fashion, despite fulfilling all other key interactions with reported essential amino acids (Table 4 of Supplementary Material). Unexpectedly, compound (**15 b**) with unsubstituted aniline moiety, exhibited considerable HDAC6 inhibition (30%), although (i) it has no linear hydrocarbon linker between the thieno[2,3-*d*]pyrimidine fragment and its hydroxamate moiety. (ii) it has a low binding affinity to HDAC6 of (-CDOCKER energy = 15.78). (iii) it could not form a coordinate bond between the hydroxamate moiety and the zinc metal. (iv) it also missed the essential hydrogen bond with HIS573 as shown in (Table 4 of Supplementary Material). Finally, future directions towards optimisation of the identified lead inhibitor (**20 b**) involve: (i) hydrocarbon linker from five to seven carbons to enhance the potency of novel thieno[2,3-*d*]pyrimidine derivatives against HDACs, to be able to capture the zinc metal in bidentate fashion with shorter distances as TSA. (ii) Hydrophobic cap group of thieno[2,3-*d*]pyrimidine derivatives bearing aniline moiety instead of the larger thieno[2,3-*d*]pyrimidine derivatives with biphenyl urea or thiourea moiety, in which it has a better binding affinity and showed higher inhibition to HDAC6.

3.3.2. In silico ADMET predictive study

A computer-aided ADMET study was performed using Accelrys Discovery Studio 4.5 software protocols to investigate pharmacokinetics properties of newly synthesised thieno[2,3-*d*] pyrimidine

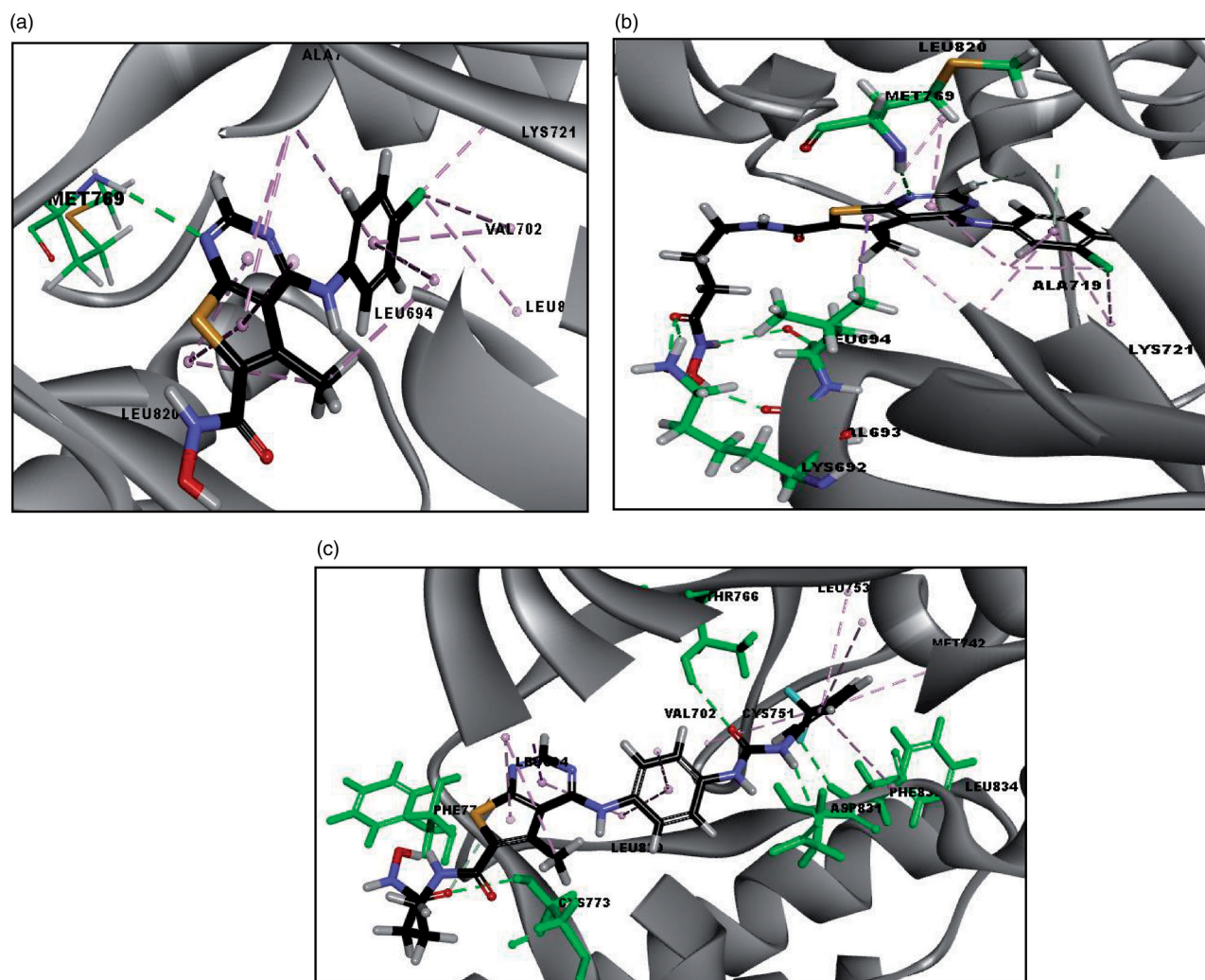


Figure 7. (a) 3D images of binding interaction of compound (15c) (-CDOCKER energy = 28.34) with EGFR (with PDB code: 4HJO), (b) 3D images of binding interaction of compounds (20d) (-CDOCKER energy = 42.52) with EGFR (c) 3D images of binding interaction of compound (12c) (-CDOCKER energy = 43.31) with EGFR. Hydrogen bond interaction is described as a green-dotted line, hydrophobic interactions are described as purple dotted lines and halogen bonds are described as cyan-dotted lines.

hydroxamic acid derivatives and their ester derivatives, such as absorption, distribution, metabolism, excretion and toxicity. This study was done to investigate the unexpected moderate *in vitro* antiproliferative activity of most of the synthesised hydroxamic acid compounds despite their potent *in vitro* EGFR and VEGFR-2 enzyme inhibition. Aqueous solubility, blood brain barrier (BBB) penetration, CYP2D6 binding, human intestinal absorption (HIA), toxicity and plasma protein binding descriptors are predicted. 2D ADMET plot for thieno[2,3-*d*] pyrimidine hydroxamic acid derivatives is drawn between ADMET_PSA_2D versus ADMET_AlogP98 (Figure 1 of Supplementary Material). Two analogous 95% and 99% confidence ellipses are shown in the biplot corresponding to HIA and BBB models⁴⁰. The results of the calculated representative parameters for thieno[2,3-*d*] pyrimidine hydroxamic acid derivatives are tabulated in (Table 5 of Supplementary Material). There is an inverse relationship between polar surface area (PSA) with percent HIA and thus cell membrane permeability⁴¹. ALogP is used to indicate the lipophilicity of the investigated compounds, thus calculating ALogP with PSA is used to bring information about hydrogen bond characteristics⁴². Optimum cell membrane permeability is predicted if the compound has (PSA < 140 Å² and AlogP98 < 5)⁴². In this study, all hydroxamic acid compounds showed AlogP98 < 5, 14 compounds showed high accepted values of PSA: 140 Å² < PSA > 100 Å², indicating considerable cell

membrane permeability but not highly permeable due to its high value of PSA (>100 Å²), which is inversely proportional with cell membrane permeability. Whereas, the rest of the compounds bearing urea moiety and with linker between the hydroxamic acid moiety and the amide connecting unit (11a-c, 12a-c) showed PSA > 140, which indicated poor cell membrane permeability and absorption.

By comparing the AlogP98 and the PSA of the synthesised thieno[2,3-*d*] pyrimidine hydroxamic acids and their esters (Table 6 of Supplementary Material), it was found that almost all of the prepared thieno[2,3-*d*]pyrimidine esters showed lower PSA (PSA < 140) and higher AlogP than most of the synthesised target thieno[2,3-*d*]pyrimidine hydroxamic acids. These results coincide with the unsatisfactory poor to moderate *in vitro* antiproliferative activities of the hydroxamic acid derivatives which could be attributed to their poor cell membrane permeability. Also, it was found that the synthesised hydroxamic acid compounds bearing aniline moiety were predicted to show better intestinal absorption and cell membrane permeability than compounds bearing urea moieties. While compounds (7a-d) bearing urea moiety with no linear hydrocarbon linker between the hydroxamic acid moiety and the thieno[2,3-*d*]pyrimidine fragment were predicted to have acceptable cell membrane permeability as an exception.

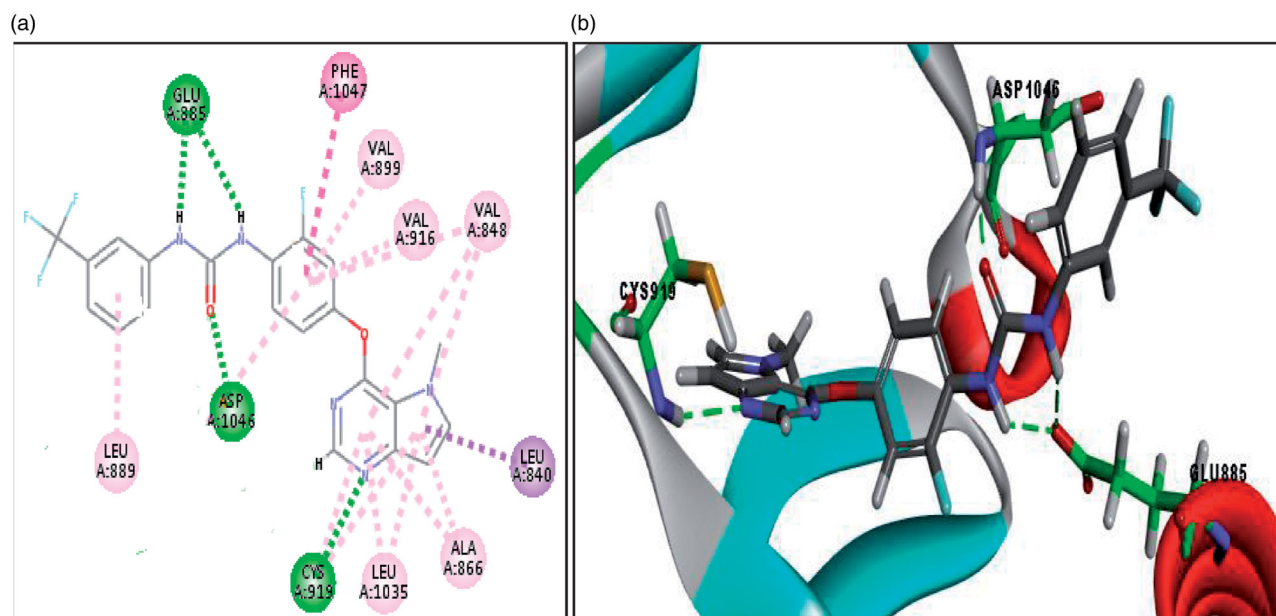


Figure 8. (a) 2D image of binding interaction of reference with VEGFR-2 (PDB code: 3VHE), (-CDOCKER energy = 42.91). (b) 3D image of binding interaction of reference with VEGFR-2 (with PDB code: 3VHE). Hydrogen bond interaction is described as a green-dotted line, hydrophobic interactions are described as purple dotted lines, Pi-Pi interaction is described as a pink-dotted line.

4. Conclusion

In the current study, series of hybrids of thieno[2,3-*d*]pyrimidine fragment bearing arylamino and diaryl urea moieties at 4-position linked to hydroxamic acid moiety were designed and synthesised as inhibitors for EGFR/VEGFR-2/HDAC6. Compounds (**12c**, **15b** and **20b**) may be considered as potential multitarget inhibitors against EGFR/VEGFR-2/HDAC6. Additionally, other synthesised novel hydroxamic acid compounds may be considered as EGFR/VEGFR-2 dual inhibitors, such as (**7a**, **15c** and **15d**), in which the hydroxamic acid moiety is directly attached to the thieno[2,3-*d*]pyrimidine fragment, contributing to maximum inhibitory dual activity. Compound (**15c**) could be the most potent dual EGFR/VEGFR-2 inhibitor in this study. Moreover, promising selective VEGFR-2 (**7c** and **11c**) and EGFR (**20d**) inhibitors were identified. The results of the enzyme inhibitory assays were found to coincide with the molecular docking studies performed on the three enzymes EGFR, VEGFR-2 and HDAC6.

These results supported the rationale of the design strategy, where the thieno[2,3-*d*]pyrimidine fragment bearing urea moiety or aniline moiety may be considered as a promising capping group. Unexpectedly, it is observed that most of the compounds showed common inhibition (weak to moderate inhibition) towards Renal UO-31 and CNS cancer SNB-75 cell lines (20–29% inhibition) although they showed potent enzyme inhibitory profiles. Results of the ADMET study revealed poor cell membrane permeability, explaining their unsatisfactory *in vitro* antiproliferative activities. Future structural modifications will be studied by implementing specific structural modifications to optimise the hydrophobicity of the designed compounds for enhancing their cell membrane permeability.

5. Experimental protocols

5.1. Chemistry

Reagents and starting materials were obtained from Alfa-Aeser organics and Sigma Aldrich without further purification. Melting points were uncorrected and recorded using BUCHI B-540

apparatus. Thin layer chromatography (TLC) is performed on 0.255 mm silica gel plates and is purchased from Merck to monitor reactions under U.V. light (254 nm). Mass spectrum was recorded in Thermo Scientific GCMS model on Direct Inlet part to mass analyser ISQ at the Regional Centre for Mycology and Biotechnology, Al-Azhar University. ^1H and ^{13}C NMR spectra were recorded on a Bruker Avance III HD FT-high resolution- NMR 400 MHz and scaled as δ in ppm at the Centre for Drug Discovery Research and Development, Faculty of Pharmacy, Ain Shams University. Description of coupling patterns is as follows: s, singlet; br s, singlet broad; d, doublet; t, triplet; m, multiplet; and 1H, 2H, 3H, etc. The coupling constants are described as *J*, which was rounded off to one decimal place. IR spectra were done at the Micro analytical centre, Cairo University, and recorded on a 4100 Jasco spectrophotometer. Elemental analysis was performed at the Regional Centre for Mycology and Biotechnology, AL Azhar University.

5.1.1. Diethyl (5-amino-3-methylthiophene)-2,4-dicarboxylate (**1**)

A solution of ethyl cyanoacetate (0.01 mol), ethyl acetoacetate (0.01 mol), sulphur (0.01 mol) and morpholine (0.01 mol) was stirred and heated (70 °C) in absolute ethanol (30 ml) for 4 h. The mixture was then left for 24 h at 0 °C. The formed solid was filtered, rinsed with ethanol (20 ml), dried and then crystallised from absolute ethanol to yield the titled compound as yellow crystals (**1**) (1.85 g, 72%), m.p. 107–109 °C (as reported)^{21,43}.

5.1.2. Ethyl (5-methyl-4-oxo-3,4-dihydrothieno[2,3-*d*]pyrimidine)-6-carboxylate (**2**)

A solution of (**1**) (2 g, 7.8 mmol) in formamide (16 ml) and acetic acid (0.5 ml) was heated under reflux at 150 °C for 40 h, cooled to 70 °C and then 90 ml water was added. The suspension was then cooled to room temperature with stirring. The formed solid was collected by filtration, washed with water (2 × 10 ml) and dried to give the titled compound as pale yellow solid (**2**) (1.8 g, 90%), m.p. 246–248 °C (as reported)^{44,45}.

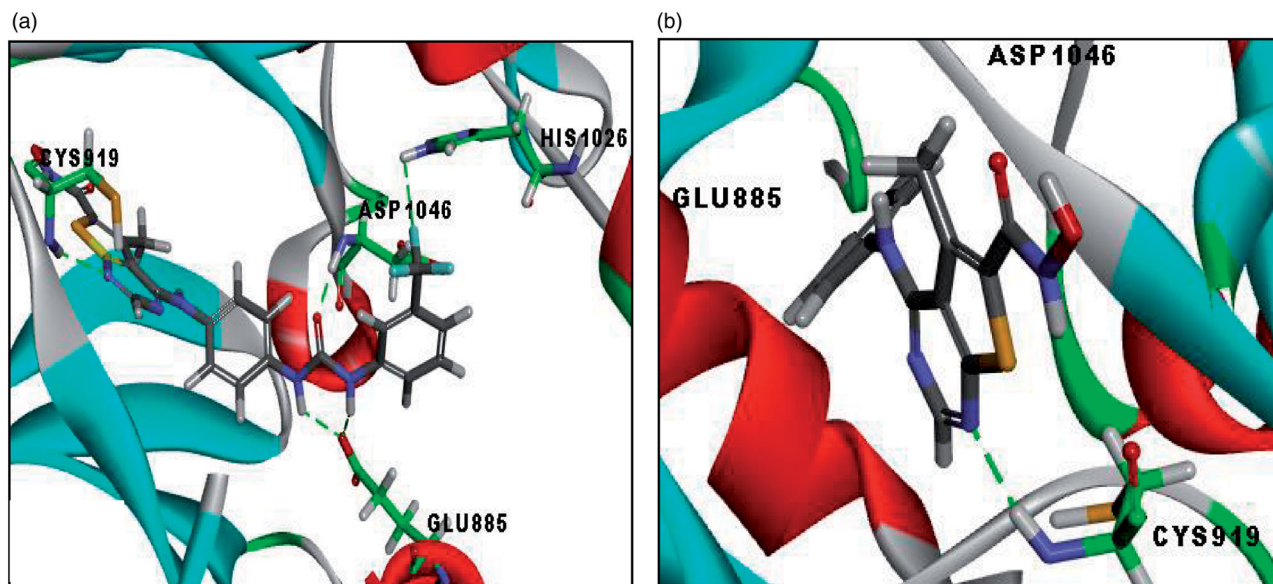


Figure 9. (a) 3D image of binding interactions of compound (7c) (-CDOCKER energy = 51.35) with VEGFR-2 (PDB code: 3VHE). (b) 3D image of binding interaction of compound (15c) (-CDOCKER energy =30.81) with VEGFR-2. Hydrogen bond interaction is described as green-dotted line.

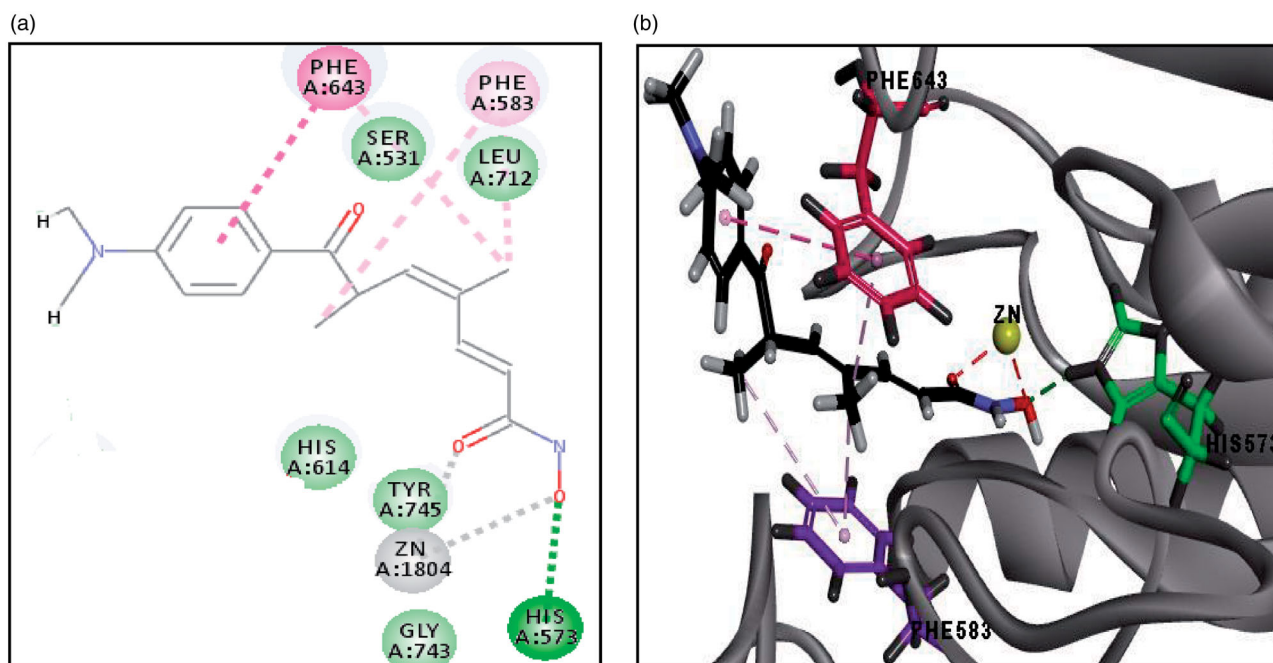


Figure 10. (a) The 2D image of binding interactions of Trichostatin A with HDAC6 (PDB code: 5G0H). (b) 3D image of binding interaction of redocked TSA with HDAC6 (-CDOCKER ENERGY= 25.54), where hydrogen bond interaction is described as green-dotted line, hydrophobic interactions are described as purple-dotted lines, pi-pi stacking is described as pink-dotted line and coordinate bond with zinc metal is described as grey-dotted line (2D image) and red-dotted line (3D image).

5.1.3. Ethyl (4-chloro-5-methylthieno[2,3-d]pyrimidine)-6-carboxylate (3)

A mixture of compound (2) (3.5 g, 14.7 mmol; 1 equiv) and phosphorus oxychloride (29 ml, 278 mmol; 18.9 equiv.) was refluxed at 90 °C for 4 h. The mixture was then slowly poured on iced cold water with continuous stirring. The formed solid was filtered off immediately and dried thoroughly over anhydrous sodium sulphate to afford the titled compound (3) (3.46 g, 92%) as light brown crystals, m.p. 114–115 °C (as reported)²².

5.1.4. General procedure for preparation of compounds (4a-d)

The appropriate isocyanate (7 mmol; 1 equiv.) was added to a solution of *p*-nitroaniline (7 mmol; 1 equiv.) in dry methylene chloride

(20 ml) and stirred at room temperature for 24 h. The formed solid was filtered, stirred again with dry methylene chloride then collected by filtration and dried. Crystallisation from ethanol yielded the titled compounds (4a-d)²³.

5.1.4.1. 1-(4-nitrophenyl)-3-phenylurea (4a). Yield 55% as yellowish white crystals, m.p. 226–228 °C (as reported)⁴⁶.

5.1.4.2. 1-(3-methoxyphenyl)-3-(4-nitrophenyl)urea (4b). Yield 50% as yellow crystals, m.p. 210–212 °C (as reported)⁴⁶.

5.1.4.3. 1-(4-nitrophenyl)-3-(3-(trifluoromethyl)phenyl)urea (4c). Yield 69% as greenish yellow crystals, m.p. 258–260 °C (as reported)³⁷.

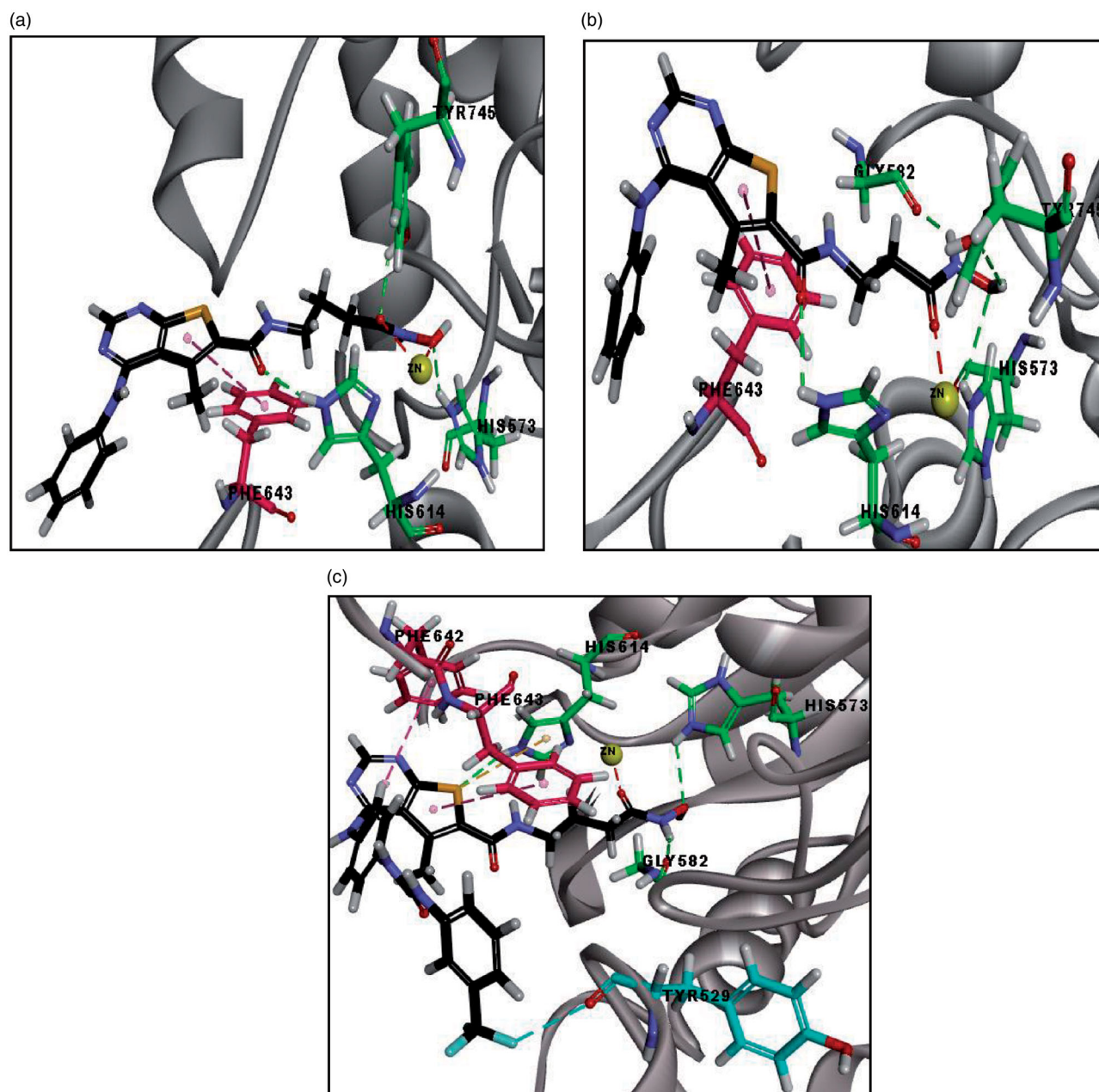


Figure 11. (a) 3D image of binding interactions of **(20b)** (-CDOCKER ENERGY= 34.32) with HDAC6 (PDB code: 5G0H). (b) 3D image of binding interaction of **(19b)** (-CDOCKER ENERGY= 37.68) with HDAC6. (c) 3D image of binding interaction of **(12c)** (-CDOCKER ENERGY= 37.58) with HDAC6. Hydrogen bond interaction is described as a green-dotted line, Pi-Pi interaction is described as a pink-dotted line, halogen interaction is described as cyan dotted lines and coordinate bond with zinc metal is described as a red dotted line.

5.1.4.4. 1-(4-nitrophenyl)-3-phenylthiourea (4d). Yield 59% as yellow crystals, m.p. 147–149 °C (as reported)⁴⁷.

5.1.5. General procedure for preparation of compounds (5a-d)

A mixture of the appropriate nitro phenyl urea or thiourea derivatives (**4a-d**) (4 mmol) and Pd-C (0.1 g, 10%) in methanol (100 ml) was stirred under H₂ at 60 bars, at room temperature for 6 h. Then Pd-C was completely removed through filtration over celite. The filtrate was evaporated under vacuum and dried to afford titled compounds (**5a-d**) which were then recrystallized from its suitable solvent²⁴.

5.1.5.1. 1-(4-aminophenyl)-3-phenylurea (5a). Yield 85%, crystallised from ethyl acetate/hexane as white crystals, m.p. 297–300 °C (as reported)⁴⁸.

5.1.5.2. 1-(3-methoxyphenyl)-3-(4-aminophenyl)urea (5b). Yield 70%, crystallised from ethanol as white crystals, m.p. 164–168 °C (as reported)³⁸.

5.1.5.3. 1-(4-aminophenyl)-3-(3-(trifluoromethyl)phenyl)urea (5c). Yield 80%, crystallised from ethanol as greyish white crystals, m.p. 148–150 °C (as reported)³⁷.

5.1.5.4. 1-(4-aminophenyl)-3-phenylthiourea (5d). Crystallised from ethanol as dark purple liquid, b.p. 410 °C (as reported)³⁰.

5.1.6. General procedure for preparation of 5-aminobenzimidazole (13a)

A mixture of 5-nitro benzimidazole (1 g, 30.65 mmol) and 10% Pd/C (0.1 g) in methanol (40 ml) was stirred under H₂ at 60 bars, at

room temperature for 6 h. The Pd/C was removed completely through filtration over celite, then the filtrate was evaporated under vacuum and dried to afford brown crystals of (**13a**) (0.84 g, 85%), m.p. 165–166 °C (as reported)⁴⁹.

5.1.7. General procedure for preparation of compounds (6a-d) and (14a-d)

To a solution of the ethyl (4-chloro-5-methylthieno[2,3-d]pyrimidine-6-carboxylate (**3**) (0.256 g, 1 mmol; 1 equiv.) in ethanol (15 ml), the appropriate amino phenyl urea and thiourea derivatives (**5a-d**)/5 amino benzimidazole derivative (**13a**)/appropriate aniline derivatives (**13 b-d**) (1 mmol; 1 equiv.) and triethylamine TEA (0.3 ml, 2 mmol; 2equiv.) were added. The mixture was heated for 24–48 h under reflux. The formed solid was filtered, washed with hot ethanol, dried, and crystallised from appropriate solvent to afford the titled compounds (**6a-d**) and (**14a-d**)²⁵.

5.1.7.1. Ethyl 5-methyl-4-(4-(3-phenylureido)phenylamino)thieno[2,3-d]pyrimidine-6-carboxylate (6a). Yield 88% as white crystals, crystallised from acetone, m.p. 319–322 °C (as reported)⁵⁰.

5.1.7.2. Ethyl 4-(4-(3-(3-methoxyphenyl)ureido)phenylamino)-5-methylthieno[2,3-d]pyrimidine-6-carboxylate (6b). Yield 84% as buff crystals, crystallised from acetone, m.p. 220–222 °C (as reported)⁵⁰.

5.1.7.3. Ethyl 4-(4-(3-(3-trifluoromethylphenyl)ureido)phenylamino)-5-methylthieno[2,3-d]pyrimidine-6-carboxylate (6c). Yield 60% as greyish white crystals, crystallised from ethanol, m.p. 305–307 °C. ¹HNMR (400 MHz, DMSO-d₆) δ: 1.32–1.36 (t, 2H, CH₂CH₃, J = 8 Hz), 3.07 (s, 3H, CH₃), 4.32–4.38 (q, 2H, CH₂CH₃, J = 8 Hz), 7.31–7.33 (d, 1H, aromatic H₆'', J = 8 Hz), 7.49–7.51 (d, 2H, aromatic H₄'', H₅'', J = 8 Hz), 7.54–7.56 (d, 2H, aromatic H₂', H₆', J = 8 Hz), 7.58–7.60 (d, 2H, aromatic H₃', H₅', J = 8 Hz), 8.04 (s, 1H, aromatic H₂''), 8.46 (s, 1H, pyrimidine H), 8.60, 8.88, 9.10 (s × 3, 3H, NH × 3, exchangeable by D₂O).

5.1.7.4. Ethyl 5-methyl-4-(4-(3-phenylthioureido)phenylamino)thieno[2,3-d]pyrimidine-6-carboxylate (6d). Yield 71% as grey solid, crystallised from ethanol, m.p. 173–175 °C. ¹HNMR (400 MHz, DMSO-d₆) δ: 1.31–1.35 (t, 2H, CH₂CH₃, J = 8 Hz), 3.02 (s, 3H, CH₃), 4.30–4.36 (q, 2H, CH₂CH₃, J = 8 Hz), 5.31 (br s, 2H, NH × 2, exchangeable by D₂O), 6.59–6.61 (d, 2H, aromatic H₂', H₆', J = 8 Hz), 7.20–7.22 (d, 2H, aromatic H₃', H₅', J = 8 Hz), 7.49–7.71 (m, 5H, aromatic H₂''- H₆''), 8.36 (s, 1H, pyrimidine H), 8.38 (s, 1H, NH, exchangeable by D₂O).

5.1.7.5. Ethyl 4-(1H-benzo[d]imidazol-5-ylamino)-5-methylthieno[2,3-d]pyrimidine-6-carboxylate. (14a). Yield 77% as faint brown crystals, crystallised from acetone, m.p. 250–251 °C (as reported)⁵⁰.

5.1.7.6. Ethyl 5-methyl-4-(phenylamino)thieno[2,3-d]pyrimidine-6-carboxylate (14b). Yield 89% as white crystals, crystallised from ethanol, m.p. 170–172 °C (as reported)⁵¹.

5.1.7.7. Ethyl 4-(4-chlorophenylamino)-5-methylthieno[2,3-d]pyrimidine-6-carboxylate (14c). Yield 82% as yellow crystals, crystallised from ethanol, m.p. 174–176 °C (as reported)⁵².

5.1.7.8. Ethyl 4-(3-chloro-4-fluorophenylamino)-5-methylthieno[2,3-d]pyrimidine-6-carboxylate (14d). Yield 97% as faint yellow crystals, crystallised from ethanol, m.p. 154–156 °C (as reported)⁵².

5.1.8. General procedure for preparation of compounds (7a-d) and (15a-d)

A cooled solution of sodium (27 mmol; 10 equiv.) in absolute ethanol (20 ml) was added to a solution of hydroxylamine hydrochloride (54 mmol; 20 equiv.) in absolute ethanol cooled in an ice bath. The mixture was stirred for 15 min. The formed precipitate was filtered, and the free hydroxylamine solution was prepared. The freshly prepared hydroxylamine solution was placed in a rounded bottom flask and cooled in an ice bath. Compounds (**6a-d**) and (**14a-d**) (2.7 mmol; 1 equiv.) were added to the solution and the mixture was stirred overnight. The reaction is monitored by TLC till the complete disappearance of starting material using an appropriate eluting system [DCM: MeOH (9.5:0.5)]. The solvent was removed under vacuum to afford crude products, washed with water and crystallised from ethanol to afford target compounds (**7a-d**) and (**15a-d**)^{26,27}.

5.1.8.1. 1-(4-(6-(hydroxycarbamoyl)-5-methylthieno[2,3-d]pyrimidin-4-ylamino)phenyl)-3-phenylurea (7a). Yield 80% as yellowish orange solid, m.p. > 200 °C. ¹HNMR (400 MHz, DMSO-d₆) δ: 3.16 (s, 3H, CH₃), 6.93–6.96 (t, 1H, aromatic H₄'', J = 8 Hz), 7.26–7.30 (t, 2H, aromatic H₂', H₆', J = 8 Hz), 7.56–7.62 (m, 6H, aromatic H₃', H₅', H₂'', H₃'', H₅'', H₆''), 8.23 (s, 1H, NH, exchangeable by D₂O), 8.38 (s, 1H, pyrimidine H), 9.81, 9.95 (s × 2, 2H, NH × 2, exchangeable by D₂O). **MS: m/z (%)**: 435 (M⁺+1, 22%), 434 (M⁺, 40%), 130 (100%). **Anal. Calcd. For C₂₁H₁₈N₆O₃S**: C 58.05, H 4.18, N 19.35, S 7.38; Found: C 58.21, H 4.35, N 19.50, S 7.46.

5.1.8.2. 1-(4-(6-(hydroxycarbamoyl)-5-methylthieno[2,3-d]pyrimidin-4-ylamino)phenyl)-3-(3-methoxyphenyl)urea (7b). Yield 75% as yellow solid, m.p. > 200 °C. ¹HNMR (400 MHz, DMSO-d₆) δ: 3.13 (s, 3H, CH₃), 3.75 (s, 3H, OCH₃), 6.52–6.54 (d, 1H, aromatic H₄'', J = 8 Hz), 7.01–7.19 (m, 3H, aromatic H₂', H₆', H₅''), 7.32 (s, 1H, aromatic H₂''), 7.49–7.60 (m, 3H, aromatic H₃', H₅', H₆'), 8.21 (s, 1H, pyrimidine H), 8.27, 8.36, 9.74, 9.79 (s × 4, 4H, NH × 4, exchangeable by D₂O), 11.13 (s, OH, exchangeable by D₂O). ¹³C NMR (DMSO-d₆, 400 MHz) δ: 14.92, 55.26, 104.21, 107.99, 112.50, 118.67, 121.01, 123.72, 133.72, 136.56, 144.23, 146.22, 149.27, 153.38, 156.91, 159.96, 162.90, 164.46, 168.44. **MS: m/z (%)**: 466 (M⁺+2, 26%), 464 (M⁺, 30%), 132 (M⁺, 100%). **Anal. Calcd. For C₂₂H₂₀N₆O₄S**: C 56.89, H 4.34, N 18.09, S 6.90; Found: C 57.15, H 4.29, N 18.30, S 6.83. **FT-IR (ú max, cm⁻¹)**: 3583 (NH stretch), 3441, 3417 (OH/NH broad), 3011 (CH aromatic), 2835–2769 (CH aliphatic), 1728 (C=O), 1635 (C=O amide), 1612 (NH bend).

5.1.8.3. 1-(4-(6-(hydroxycarbamoyl)-5-methylthieno[2,3-d]pyrimidin-4-ylamino)phenyl)-3-(3-(trifluoromethyl)phenyl)urea (7c). Yield 69% as yellow solid, m.p. 285 °C. ¹HNMR (400 MHz, DMSO-d₆) δ: 3.07 (s, 3H, CH₃), 3.16 (s, 1H, OH, exchangeable by D₂O), 7.29–7.31 (d, 1H, aromatic H₆'', J = 8 Hz), 7.50–7.55 (m, 2H, aromatic H₄'', H₅''), 7.59–7.61 (d, 2H, aromatic H₂', H₆', J = 8 Hz), 7.66–7.68 (d, 2H, aromatic H₃', H₅', J = 8 Hz), 8.09 (s, 1H, aromatic H₂''), 8.30 (s, 1H, pyrimidine H), 8.39, 8.47, 8.61, 9.59 (s × 4, 4H, NH × 4, exchangeable by D₂O). **MS: m/z (%)**: 502 (M⁺, 24%), 286 (94%), 211 (100%). **Anal. Calcd. For C₂₂H₁₇F₃N₆O₃S**: C 52.59, H 3.41, N 16.73, S 6.38; Found: C 52.57, H 3.40, N 16.71, S 6.38.

5.1.8.4. *1-(4-(6-(hydroxycarbamoyl)-5-methylthieno[2,3-d]pyrimidin-4-ylamino)phenyl)-3-phenylthiourea (7d)*. Yield 65% as brown solid, m.p 300 °C. ¹HNMR (400 MHz, DMSO-d₆) δ: 1.24 (s, 1H, OH, exchangeable by D₂O), 3.04 (s, 3H, CH₃), 4.94 (s, 1H, NH, exchangeable by D₂O), 6.56–6.58 (d, 2H, aromatic H_{2'}, H_{6'}, J=8 Hz), 7.22–7.24 (d, 2H, aromatic H_{3'}, H_{5'}, J=8 Hz), 7.55–7.99 (m, 5H, aromatic H_{2''}-H_{6''}), 8.23 (s, 1H, pyrimidine H), 8.54 (s, 1H, NH, exchangeable by D₂O). **MS: m/z (%)**: 450 (M⁺, 28%), 448 (M⁺², 13%), 240 (100%). **Anal. Calcd. For C₂₁H₁₈N₆O₂S₂**: C 55.98, H 4.03, N 18.65, S 14.23; Found: C 56.11, H 4.28, N 18.71, S 14.09. **FT-IR (ú max, cm⁻¹)**: 3433 (OH/NH broad), 3016 (CH aromatic), 2958–2854 (CH aliphatic), 1732 (C=O), 1658 (C=O amide), 1612 (NH bend).

5.1.8.5. *4-(1H-benzo[d]imidazol-4-ylamino)-N-hydroxy-5-methylthieno[2,3-d]pyrimidine-6-carboxamide (15a)*. Yield 89% as orange brown solid, m.p 280 °C. ¹HNMR (400 MHz, DMSO-d₆) δ: 2.94 (s, 3H, CH₃), 5.42 (s, 1H, NH, exchangeable by D₂O), 7.37–7.39 (d, 1H, aromatic H_{5'}, J=8 Hz), 7.58–7.60 (d, 1H, aromatic H_{4'}, J=8 Hz), 7.98 (s, 1H, aromatic H_{7'}), 8.21 (s, 1H, aromatic H_{2'}), 8.41 (s, 1H, pyrimidine H), 8.53, 8.58 (s, 2H, NH × 2, exchangeable by D₂O). **MS: m/z (%)**: 340 (M⁺, 65%), 341 (M⁺¹, 11%), 102 (100%). **Anal. Calcd. For C₁₅H₁₂N₆O₂S**: C 52.93, H 3.55, N 24.69, S 9.42; Found: C 53.17, H 3.64, N 24.58, S 9.53. **FT-IR (ú max, cm⁻¹)**: 3441 (OH broad), 3417, 3398 (2 × NH stretch), 3170–3113 (CH aromatic), 2958–2854 (CH aliphatic), 1662 (C=O), 1573 (NH bend).

5.1.8.6. *N-hydroxy-5-methyl-4-(phenylamino)thieno[2,3-d]pyrimidine-6-carboxamide (15b)*. Yield 90% as greyish brown, m.p 200 °C. ¹HNMR (400 MHz, DMSO-d₆) δ: 2.92 (s, 1H, OH, exchangeable by D₂O), 3.08 (s, 3H, CH₃), 7.08–7.14 (m, 1H, aromatic H_{4'}), 7.34–7.38 (t, 2H, aromatic H_{2'}, H_{6'}, J=8 Hz), 7.66–7.70 (t, 2H, aromatic H_{3'}, H_{5'}, J=8 Hz), 8.31, 8.39 (s × 2, 2H, NH × 2, exchangeable by D₂O), 8.43 (s, 1H, pyrimidine H). **MS: m/z (%)**: 300 (M⁺, 29%), 301 (M⁺¹, 19%), 195 (100%). **Anal. Calcd. For C₁₄H₁₂N₄O₂S**: C 55.99, H 4.03, N 18.65, S 10.68; Found: C 56.16, H 4.29, N 18.78, S 10.81. **FT-IR (ú max, cm⁻¹)**: 3452 (NH stretch), 3394 (OH/NH broad), 3010 (CH aromatic), 2978–2862 (CH aliphatic), 1600 (C=O), 1566 (NH bend).

5.1.8.7. *4-(4-chlorophenylamino)-N-hydroxy-5-methylthieno[2,3-d]pyrimidine-6-carboxamide (15c)*. Yield 95% as yellow solid, m.p 349 °C. ¹HNMR (400 MHz, DMSO-d₆) δ: 3.04 (s, 3H, CH₃), 7.40–7.42 (d, 2H, aromatic H_{2'}, H_{6'}, J=8 Hz), 7.73–7.75 (d, 1H, aromatic H_{3'}, H_{5'}, J=8 Hz), 8.37 (s, 1H, NH, exchangeable by D₂O), 8.40 (s, 1H, pyrimidine H). **MS: m/z (%)**: 335 (M⁺¹, 5%), 334 (M⁺, 11%), 274 (100%). **Anal. Calcd. For C₁₄H₁₁ClN₄O₂S**: C 50.23, H 3.31, N 16.74, S 9.58; Found: C 50.18, H 3.28, N 16.73, S 9.55.

5.1.8.8. *4-(3-chloro-4-fluorophenylamino)-N-hydroxy-5-methylthieno[2,3-d]pyrimidine-6-carboxamide (15d)*. Yield 91% as buff solid, m.p 320 °C. ¹HNMR (400 MHz, DMSO-d₆) δ: 1.72 (s, 1H, OH, exchangeable by D₂O), 3.07 (s, 3H, CH₃), 7.39–7.44 (t, 1H, aromatic H_{5'}, J=8 Hz), 7.65–7.69 (m, 1H, aromatic H_{2'}), 7.96–7.99 (dd, 1H, aromatic H_{6'}, J=4, 12 Hz), 8.41 (s, NH, exchangeable by D₂O), 8.42 (s, 1H, pyrimidine H), 8.50 (s, 1H, NH, exchangeable by D₂O). **MS: m/z (%)**: 354 (M⁺², 20%), 353 (M⁺¹, 10%), 352 (M⁺, 100%). **Anal. Calcd. For C₁₄H₁₀FCIN₄O₂S**: C 47.67, H 2.86, N 15.88, S 9.09; Found: C 47.80, H 3.12, N 16.15, S 9.23. **FT-IR (ú max, cm⁻¹)**: 3441 (OH/NH broad), 2985 (CH aromatic), 2916–2769 (CH aliphatic), 1612 (C=O), 1573 (NH bend).

5.1.9. General procedure for preparation of compounds (8a-c, 16b-d)

An aqueous solution of lithium hydroxide (30 mmol) in water (50 ml) was added to a solution of compounds (**6a-c**, **14b-d**) (10 mmol) in THF (30 ml) and ethanol (9 ml). The mixture is stirred for 7 h at 50–60 °C. Complete hydrolysis is monitored by TLC, followed by the addition of ethyl acetate (50 ml), 1 N HCl (10 ml) and water (20 ml). The aqueous layer was separated from the organic layer and washed with ethyl acetate (2 × 50 ml). Then, the combined organic solutions were dried over anhydrous sodium sulphate (20 g), filtered and removed under vacuum to afford titled compounds (**8a-c**, **16b-d**)²⁸.

5.1.9.1. *5-methyl-4-(4-(3-phenylureido)phenylamino)thieno[2,3-d]pyrimidine-6-carboxylic acid (8a)*. Yield 90% as white crystals, m.p 281–283 °C (as reported)⁵⁰.

5.1.9.2. *4-(4-(3-(3-methoxyphenyl)ureido)phenylamino)-5-methylthieno[2,3-d]pyrimidine-6-carboxylic acid (8b)*. Yield 85% as white crystals, m.p 260–263 °C (as reported)⁵⁰.

5.1.9.3. *5-methyl-4-(4-(3-(3-(trifluoromethyl)phenyl)ureido)phenylamino)thieno[2,3-d]pyrimidine-6-carboxylic acid (8c)*. Yield 74% as yellow crystals, m.p. 223–225 °C. ¹HNMR (400 MHz, DMSO-d₆) δ: 3.06 (s, 3H, CH₃), 7.29–7.31 (d, 1H, aromatic H_{6''}, J=8 Hz), 7.49–7.51 (d, 2H, aromatic H_{4''}, H_{5''}, J=8 Hz), 7.54–7.56 (d, 2H, aromatic H_{2'}, H_{6'}, J=8 Hz), 7.58–7.60 (d, 2H, aromatic H_{3'}, H_{5'}, J=8 Hz), 8.03 (s, 1H, aromatic H_{2''}), 8.46 (s, 1H, pyrimidine H), 8.63, 9.05, 9.31 (s × 3, 3H, NH × 3, exchangeable by D₂O).

5.1.9.4. *5-methyl-4-(phenylamino)thieno[2,3-d]pyrimidine-6-carboxylic acid (16b) [53]*. Yield 99% as buff crystals, m.p. 178–180 °C.

5.1.9.5. *4-(4-chlorophenylamino)-5-methylthieno[2,3-d]pyrimidine-6-carboxylic acid (16c)*. Yield 89% as off white crystals, m.p 316–318 °C (as reported)⁵².

5.1.9.6. *4-(3-chloro-4-fluorophenylamino)-5-methylthieno[2,3-d]pyrimidine-6-carboxylic acid (16d)*. Yield 84% as white crystals, m.p 305–307 °C (as reported)⁵².

5.1.10. General procedure for preparation of compounds (9a-c, 17b-d)

To a solution of beta-alanine ethyl ester hydrochloride (8.94 mmol), thieno[2,3-d]pyrimidine-6-carboxylic acid derivatives (**8a-c**, **16b-d**) (8.94 mmol) and 1-hydroxybenzotriazole (1.32 g, 9.18 mmol) in dry dimethylformamide (20 ml), N-methyl morpholine (4.51 g, 44.65 mmol) was added at 0 °C and stirred for 30 min. Then EDCl.HCl (1.8 g, 13.12 mmol) was added and stirred for another 30 min maintaining the same temperature. The reaction mixture was stirred for 8 h at room temperature and then followed by the addition of water (20 ml) and ethyl acetate (2 × 20 ml) for extraction. Organic extracts were combined, washed with water (2 × 10 ml) and aqueous sodium bicarbonate solution (2 × 10 ml). Then organic solution was dried with anhydrous Na₂SO₄ and evaporated under vacuum to afford the titled compounds (**9a-c**, **17b-d**)²⁹.

5.1.10.1. *Ethyl 3-(5-methyl-4-(4-(3-phenylureido)phenylamino)thieno[2,3-d]pyrimidine-6-carboxamido)propanoate (9a)*. Yield

84% as white solid, m.p 229 °C. **¹HNMR (400 MHz, DMSO-d₆) δ:** 1.20–1.23 (t, 3H, OCH₂CH₃, J=8 Hz), 2.59–2.62 (t, 2H, CH₂CO, J=8 Hz), 2.86 (s, 3H, CH₃), 3.48–3.53 (q, 2H, CH₂NH, J=8 Hz), 4.07–4.13 (q, 2H, OCH₂CH₃, J=8 Hz), 6.96–7.00 (t, 1H, aromatic H₄'', J=8 Hz), 7.27–7.31 (t, 2H, aromatic H₂', H₆', J=8 Hz), 7.45–7.48 (d, 4H, aromatic H₂'', H₃'', H₅'', H₆'', J=12 Hz), 7.52–7.54 (d, 2H, aromatic H₃', H₅', J=8 Hz), 8.41 (s, 1H, pyrimidine H), 8.44, 8.50, 8.66, 8.69 (s × 4, 4H, NH × 4, exchangeable by D₂O). **MS: m/z (%)**: 518 (M⁺, 36%), 515 (M⁺-3, 2%), 92 (100%). **Anal. Calcd. For C₂₆H₂₆N₆O₄S:** C 60.22, H 5.05, N 16.21, S 6.18; Found: C 60.08, H 5.17, N 16.48, S 6.09.

5.1.10.2. Ethyl 3-(4-(4-(3-(3-methoxyphenyl)ureido)phenylamino)-5-methylthieno[2,3-d]pyrimidine-6-carboxamido)propanoate (9b). Yield 89% as buff solid, m.p 250 °C. **¹HNMR (400 MHz, DMSO-d₆) δ:** 1.20–1.23 (t, 3H, OCH₂CH₃, J=8 Hz), 2.59–2.62 (t, 2H, CH₂CO, J=8 Hz), 2.86 (s, 3H, CH₃), 3.48–3.53 (q, 2H, CH₂NH, J=8 Hz), 3.74 (s, 3H, OCH₃), 4.07–4.13 (q, 2H, OCH₂CH₃, J=8 Hz), 6.55–6.57 (d, 1H, aromatic H₄'', J=8 Hz), 6.93–6.95 (d, 1H, aromatic H₅'', J=8 Hz), 7.16–7.20 (t, 2H, aromatic H₂'', H₆'', J=8 Hz), 7.45–7.47 (d, 2H, aromatic H₂', H₆', J=8 Hz), 7.52–7.54 (d, 2H, aromatic H₃', H₅', J=8 Hz), 8.41 (s, 1H, pyrimidine H), 8.44, 8.50, 8.71, 10.08 (s × 4, 4H, NH × 4, exchangeable by D₂O). **MS: m/z (%)**: 546 (M⁺, 66%), 548 (M⁺+2, 67%), 501 (100%). **Anal. Calcd. For C₂₇H₂₈N₆O₅S:** C 59.11, H 5.14, N 15.32, S 5.84; Found: C 59.37, H 5.31, N 15.49, S 6.02.

5.1.10.3. Ethyl 3-(5-methyl-4-(4-(3(trifluoromethyl)phenyl)ureido)phenylamino)thieno[2,3-d]pyrimidine-6-carboxamido)propanoate (9c). Yield 85% as grey solid, m.p 220 °C. **¹HNMR (400 MHz, DMSO-d₆) δ:** 1.17–1.21 (t, 3H, OCH₂CH₃, J=8 Hz), 2.58–2.61 (t, 2H, CH₂CO, J=8 Hz), 3.01 (s, 3H, CH₃), 3.71–3.78 (q, 2H, CH₂NH, J=8 Hz), 4.17–4.23 (q, 2H, OCH₂CH₃, J=8 Hz), 7.29–7.31 (d, 1H, aromatic H₅'', J=8 Hz), 7.53–7.64 (m, 5H, aromatic H₂', H₃', H₅', H₆', H₄''), 8.01 (s, 1H, NH, exchangeable by D₂O), 8.31–8.43 (m, 3H, aromatic H₂'', H₆'' and pyrimidine H), 8.86, 9.11 (s × 2, 2H, NH × 2, exchangeable by D₂O). **MS: m/z (%)**: 587 (M⁺+1, 17%), 586 (M⁺, 55%), 77 (100%). **Anal. Calcd. For C₂₇H₂₅F₃N₆O₄S:** C 55.28, H 4.30, N 14.33, S 5.47; Found: C 55.22, H 4.27, N 14.30, S 5.45.

5.1.10.4. Ethyl 3-(5-methyl-4-(phenylamino)thieno[2,3-d]pyrimidine-6-carboxamido)propanoate (17b). Yield 95% as light brown solid, m.p 206 °C. **¹HNMR (400 MHz, DMSO) δ:** 1.19–1.23 (t, 3H, OCH₂CH₃, J=8 Hz), 2.59–2.62 (t, 2H, CH₂CO, J=8 Hz), 2.86 (s, 3H, CH₃), 3.48–3.53 (q, 2H, CH₂NH, J=8 Hz), 4.07–4.12 (q, 2H, OCH₂CH₃, J=8 Hz), 7.14–7.17 (t, 1H, aromatic H₄', J=8 Hz), 7.37–7.41 (t, 2H, aromatic H₃', H₅', J=8 Hz), 7.64–7.66 (d, 2H, aromatic H₂', H₆', J=8 Hz), 8.45 (s, 1H, pyrimidine H), 8.51 (s, 1H, NH, exchangeable by D₂O). **MS: m/z (%)**: 385 (M⁺+1, 7%), 384 (M⁺, 28%), 77 (100%). **Anal. Calcd. For C₁₉H₂₀N₄O₃S:** C 59.36, H 5.24, N 14.57, S 8.34; Found: C 59.48, H 5.37, N 14.49, S 8.47. **FT-IR (ú max, cm⁻¹):** 3452, 3224 (2 × NH stretch), 3047–3020 (CH aromatic), 2985–2904 (CH aliphatic), 1724 (C=O ester), 1651 (C=O amide), 1608 (NH bend).

5.1.10.5. Ethyl 3-(4-(4-chlorophenylamino)-5-methylthieno[2,3-d]pyrimidine-6-carboxamidopropanoate (17c). Yield 90% as buff solid, m.p 202 °C. **¹HNMR (400 MHz, CDCl₃) δ:** 1.29–1.34 (t, 3H, OCH₂CH₃, J=8 Hz), 2.67–2.70 (t, 2H, CH₂CO, J=8 Hz), 3.02 (s, 3H, CH₃), 3.69–3.77 (m, 2H, CH₂NH), 4.19–4.24 (q, 2H, OCH₂CH₃, J=8 Hz), 6.78 (s, 1H, NH, exchangeable by D₂O), 7.38–7.40 (d, 2H, aromatic H₂', H₆', J=8 Hz), 7.55 (s, 1H, NH, exchangeable by D₂O),

7.63–7.65 (d, 1H, aromatic H₃', H₅', J=8 Hz), 8.57 (s, 1H, pyrimidine H). **MS: m/z (%)**: 420 (M⁺+2, 10%) & base peak at 418 (M⁺, 100%). **Anal. Calcd. For C₁₉H₁₉ClN₄O₃S:** C 54.48, H 4.57, N 13.37, S 7.65; Found: C 54.65, H 4.80, N 13.48, S 7.78.

5.1.10.6. Ethyl 3-(4-(3-chloro-4-fluorophenylamino)-5-methylthieno[2,3-d]pyrimidine-6-carboxamido)propanoate (17d). Yield 92% as buff solid, m.p 184 °C. **¹HNMR (400 MHz, CDCl₃) δ:** 1.30–1.34 (t, 3H, OCH₂CH₃, J=8.8 Hz), 2.67–2.71 (t, 2H, CH₂CO, J=8 Hz), 3.04 (s, 3H, CH₃), 3.73–3.77 (q, 2H, CH₂NH, J=8 Hz), 4.19–4.25 (q, 2H, OCH₂CH₃, J=8.8 Hz), 6.73 (s, 1H, NH, exchangeable by D₂O), 7.19–7.23 (t, 1H, aromatic H₅', J=8 Hz), 7.51 (s, 1H, aromatic H₂'), 7.87–7.89 (d, 1H, aromatic H₆', J=8 Hz), 8.60 (s, 1H, pyrimidine H). **MS: m/z (%)**: 437 (M⁺+1, 18%), 436 (M⁺, 26%), 285 (100%). **Anal. Calcd. For C₁₉H₁₈ClFN₄O₃S:** C 52.23, H 4.15, N 12.82, S 7.34; Found: C 52.40, H 4.28, N 13.09, S 7.46. **FT-IR (ú max, cm⁻¹):** 3444, 3367 (2 × NH stretch), 3120 (CH aromatic), 2981–2858 (CH aliphatic), 1728 (C=O ester), 1639 (C=O amide), 1612 (NH bend).

5.1.11. General procedure for preparation of compounds (10a-c, 18b-d)

To a solution of ethyl 4-amino butyrate hydrochloride (8.94 mmol), prepared thieno[2,3-d]pyrimidine-6-carboxylic acid derivatives (**8a-c**, **16b-d**) (8.94 mmol) and 1-hydroxybenzotriazole (1.32 g, 9.18 mmol) in dry dimethylformamide (20 ml), N-methyl morpholine (4.51 g, 44.65 mmol) was added at 0 °C and stirred for 30 min. Then, EDCI.HCl (1.8 g, 13.12 mmol) was added and stirred for another 30 min maintaining the same temperature. The reaction mixture was stirred for 8 h at room temperature and then followed by the addition of water (20 ml) and ethyl acetate (2 × 20 ml) for extraction. Organic extracts were combined, washed with water (2 × 10 ml) and aqueous sodium bicarbonate solution (2 × 10 ml). Then the organic solution was dried with anhydrous Na₂SO₄, and evaporated under vacuum to afford the titled compounds (**10a-c**, **18b-d**)²⁹.

5.1.11.1. Ethyl 4-(5-methyl-4-(4-(3-phenylureido)phenylamino)-thieno[2,3-d]pyrimidine-6-carboxamido)butanoate (10a). Yield 84% as greyish white solid, m.p 219–221 °C. **¹HNMR (400 MHz, DMSO-d₆) δ:** 1.19–1.22 (t, 3H, OCH₂CH₃, J=8 Hz), 1.77–1.84 (m, 2H, CH₂CH₂CH₂), 2.36–2.40 (t, 2H, CH₂CO, J=8 Hz), 2.88 (s, 3H, CH₃), 3.26–3.32 (q, 2H, CH₂NH, J=8 Hz), 4.05–4.10 (q, 2H, OCH₂CH₃, J=8 Hz), 6.96–6.99 (t, 1H, aromatic H₄'', J=7.6 Hz), 7.27–7.31 (t, 2H, aromatic H₂', H₆', J=8 Hz), 7.46–7.48 (d, 4H, aromatic H₂'', H₃'', H₅'', H₆''), 7.52–7.54 (d, 2H, aromatic H₃', H₅', J=8 Hz), 8.41 (s, 1H, pyrimidine H), 8.43, 8.46, 8.68, 8.71 (s × 4, 4H, NH × 4, exchangeable by D₂O). **MS: m/z (%)**: 532 (M⁺, 28%), 530 (M⁺-2, 14%), 452 (100%). **Anal. Calcd. For C₂₇H₂₈N₆O₄S:** C 60.89, H 5.30, N 15.78, S 6.02; Found: C 60.75, H 5.43, N 16.01, S 6.14.

5.1.11.2. Ethyl 4-(4-(4-(3-(3-methoxyphenyl)ureido)phenylamino)-5-methylthieno[2,3-d]pyrimidine-6-carboxamido)butanoate (10b). Yield 80% as yellow solid, m.p 193 °C. **¹HNMR (400 MHz, DMSO-d₆) δ:** 1.18–1.22 (t, 3H, OCH₂CH₃, J=8 Hz), 1.77–1.84 (m, 2H, CH₂CH₂CH₂), 2.36–2.40 (t, 2H, CH₂CO, J=8 Hz), 2.88 (s, 3H, CH₃), 3.26–3.32 (q, 2H, CH₂NH, J=8 Hz), 3.74 (s, 3H, OCH₃), 4.05–4.11 (q, 2H, OCH₂CH₃, J=8 Hz), 6.54–7.56 (d, 1H, aromatic H₄'', J=8 Hz), 6.94–6.96 (d, 1H, aromatic H₅'', J=8 Hz), 7.16–7.21 (m, 2H, aromatic H₂'', H₆''), 7.46–7.49 (d, 2H, aromatic H₂', H₆', J=12 Hz), 7.51–7.54 (d, 2H, aromatic H₃', H₅', J=12 Hz), 8.41 (s, 1H,

pyrimidine H), 8.43, 8.46, 8.89, 8.98 ($s \times 4$, 4H, NH $\times 4$, exchangeable by D₂O). **MS: m/z (%)**: 562 (M⁺, 41%), 530 (M⁺-2, 20%), 256 (100%). **Anal. Calcd. For C₂₈H₃₀N₆O₅S**: C 59.77, H 5.37, N 14.94, S 5.70; Found: C 59.64, H 5.48, N 15.12, S 5.78.

5.1.11.3. Ethyl 4-(5-methyl-4-(4-(3-(3-(trifluoromethyl)phenyl)ureido)phenylamino)thieno[2,3-d]pyrimidine-6-carboxamido)butanoate (10c). Yield 68% as yellowish white solid, m.p 197–199 °C. **¹HNMR (400 MHz, DMSO-d₆)** δ : 1.18–1.22 (t, 3H, OCH₂CH₃, $J=8$ Hz), 1.77–1.84 (m, 2H, CH₂CH₂CH₂), 2.36–2.40 (t, 2H, CH₂CO, $J=8$ Hz), 2.88 (s, 3H, CH₃), 3.26–3.32 (q, 2H, CH₂NH, $J=8$ Hz), 4.05–4.10 (q, 2H, OCH₂CH₃, $J=8$ Hz), 7.31–7.32 (d, 1H, aromatic H₅'', $J=8$ Hz), 7.48–7.60 (m, 7H, aromatic H₂', H₃', H₅', H₆', H₂'', H₄'', H₆''), 8.05 (s, 1H, NH, exchangeable by D₂O), 8.42–8.44 (m, 2H, pyrimidine H & NH, exchangeable by D₂O), 8.88, 9.11 ($s \times 2$, 2H, NH $\times 2$, exchangeable by D₂O). **MS: m/z (%)**: 600 (M⁺, 28%), 601 (M⁺+1, 28%), 77 (100%). **Anal. Calcd. For C₂₈H₂₇F₃N₆O₄S**: C 55.99, H 4.53, N 13.99, S 5.34; Found: C 56.18, H 4.76, N 14.21, S 5.28. **FT-IR** (ν max, cm⁻¹): 3375, 3356, 3271 (3 \times NH stretch), 3155–3070 (CH aromatic), 2978–2873 (CH aliphatic), 1712 (C=O ester), 1643 (C=O amide), 1612 (NH bend).

5.1.11.4. Ethyl 4-(5-methyl-4-(phenylamino)thieno[2,3-d]pyrimidine-6-carboxamido)butanoate (18 b). Yield 94% as off white solid, m.p 145–147 °C. **¹HNMR (400 MHz, CDCl₃)** δ : 1.27–1.31 (t, 3H, OCH₂CH₃, $J=8$ Hz), 1.97–2.04 (m, 2H, CH₂CH₂CH₂), 2.46–2.50 (t, 2H, CH₂CO, $J=8$ Hz), 3.05 (s, 3H, CH₃), 3.50–3.55 (q, 2H, CH₂NH, $J=8$ Hz), 4.16–4.21 (q, 2H, OCH₂CH₃, $J=6.8$ Hz), 6.38 (s, 1H, NH, exchangeable by D₂O), 7.20–7.24 (t, 1H, aromatic H₄', $J=8$ Hz), 7.42–7.46 (t, 2H, aromatic H₃', H₅', $J=8$ Hz), 7.67–7.69 (d, 2H, aromatic H₂', H₆', $J=8$ Hz), 8.59 (s, 1H, pyrimidine H). **MS: m/z (%)**: 398 (M⁺, 15%), 399 (M⁺+1, 4%), 130 (100%). **Anal. Calcd. For C₂₀H₂₂N₄O₃S**: C 60.28, H 5.56, N 14.06, S 8.05; Found: C 60.41, H 5.75, N 14.32, S 8.19.

5.1.11.5. Ethyl 4-(4-(4-chlorophenylamino)-5-methylthieno[2,3-d]pyrimidine-6-carboxamido)butanoate (18c). Yield 96% as pale yellow solid, m.p 138 °C. **¹HNMR (400 MHz, DMSO)** δ : 1.18–1.22 (t, 3H, OCH₂CH₃, $J=8$ Hz), 1.76–1.84 (m, 2H, CH₂CH₂CH₂), 2.36–2.40 (t, 2H, CH₂CO, $J=8$ Hz), 2.87 (s, 3H, CH₃), 3.26–3.31 (q, 2H, CH₂NH, $J=8$ Hz), 4.05–4.10 (q, 2H, OCH₂CH₃, $J=8$ Hz), 7.43–7.45 (d, 2H, aromatic H₂', H₆', $J=8$ Hz), 7.69–7.71 (d, 1H, aromatic H₃', H₅', $J=8$ Hz), 8.47 (br s, 1H, NH, exchangeable by D₂O), 8.49 (s, 1H, pyrimidine H), 8.59 (s, 1H, NH, exchangeable by D₂O). **MS: m/z (%)**: 433 (M⁺+1, 36%), 434 (M⁺+2, 35%), 432 (M⁺, 100%). **Anal. Calcd. For C₂₀H₂₁ClN₄O₃S**: C 55.49, H 4.89, N 12.94, S 7.41; Found: C 55.38, H 5.12, N 12.87, S 7.48.

5.1.11.6. Ethyl 4-(4-(3-chloro-4-fluorophenylamino)-5-methylthieno[2,3-d]pyrimidine-6-carboxamido)butanoate (18d). Yield 90% as faint yellow solid, m.p 131–133 °C. **¹HNMR (400 MHz, DMSO-d₆)** δ : 1.18–1.21 (t, 3H, OCH₂CH₃, $J=8$ Hz), 1.77–1.84 (m, 2H, CH₂CH₂CH₂), 2.36–2.40 (t, 2H, CH₂CO, $J=8$ Hz), 2.87 (s, 3H, CH₃), 3.26–3.32 (q, 2H, CH₂NH, $J=8$ Hz), 4.05–4.10 (q, 2H, OCH₂CH₃, $J=8$ Hz), 7.43–7.47 (t, 1H, aromatic H₅', $J=8$ Hz), 7.63–7.67 (m, 1H, aromatic H₂'), 7.92–7.94 (dd, 1H, aromatic H₆', $J=2.8, 6.8$ Hz), 8.48 (s, 1H, NH, exchangeable by D₂O), 8.50 (s, 1H, pyrimidine H), 8.60 (s, 1H, NH, exchangeable by D₂O). **MS: m/z (%)**: 450 (M⁺, 30%), 434 (M⁺+2, 35%), 110 (100%), 66 (85%). **Anal. Calcd. For C₂₀H₂₀ClF₂N₄O₃S**: C 53.27, H 4.47, N 12.43, S 7.11; Found: C 53.49, H 4.61, N 12.69, S 7.17.

5.1.12. General procedure for preparation of compounds (11a-c, 19b-d, 12a-c and 20b-d)

A cooled solution of sodium (27 mmol; 10 equiv.) in absolute ethanol (20 ml) was added to a solution of hydroxylamine hydrochloride (54 mmol; 20 equiv.) in absolute ethanol cooled in an ice bath. The mixture was stirred for 15 min. The formed precipitate was filtered, and the free hydroxylamine solution was prepared. The freshly prepared hydroxylamine solution was placed in a rounded bottom flask and cooled in an ice bath. Compounds (9a-c, 17 b-d, 10a-c, 18 b-d) (2.7 mmol; 1 equiv.) were added to the solution and stirred overnight. The reaction is monitored by TLC till the complete disappearance of starting compounds using an appropriate eluting system [DCM: MeOH (9.5:0.5)]. The solvent was removed under vacuum to afford crude products, washed with water, and crystallised from ethanol to yield target compounds (11a-c, 19 b-d, 12a-c, 20b-d)^{26,27}.

5.1.12.1. 1-(4-(6-((3-(hydroxyamino)-3-oxopropyl)carbamoyl)-5-methylthieno[2,3-d]pyrimidin-4-ylamino)phenyl)-3-phenylurea

(11a). Yield 80% as yellow solid, m.p 225 °C. **¹HNMR (400 MHz, DMSO-d₆)** δ : 2.36–2.39 (t, 2H, CH₂CO, $J=8$ Hz), 2.90 (s, 3H, CH₃), 3.47–3.52 (q, 2H, CH₂NH, $J=8$ Hz), 6.88–6.91 (t, 1H, aromatic H₄'', $J=8$ Hz), 7.20–7.28 (m, 4H, aromatic H₂', H₆', H₃'', H₅''), 7.23–7.25 (d, 2H, aromatic H₂', H₆', $J=8$ Hz), 7.50–7.52 (d, 2H, aromatic H₃', H₅', $J=8$ Hz), 7.58–7.60 (d, 2H, aromatic H₂'', H₆'', $J=8$ Hz), 8.14 (s, 1H, NH, exchangeable by D₂O), 8.28 (s, 1H, pyrimidine H), 8.40, 9.09, 9.42, 10.89 ($s \times 4$, 4H, NH $\times 4$, exchangeable by D₂O), 11.01 (s, 1H, OH, exchangeable by D₂O). **MS: m/z (%)**: 505 (M⁺, 28%), 504 (M⁺-1, 36%), 306 (100%). **Anal. Calcd. For C₂₄H₂₃N₇O₄S**: C 57.02, H 4.59, N 19.39, S 6.34; Found: C 57.21, H 4.80, N 19.47, S 6.41.

5.1.12.2. 1-(4-(6-((3-(hydroxyamino)-3-oxopropyl)carbamoyl)-5-methylthieno[2,3-d]pyrimidin-4-ylamino)phenyl)-3-(3-methoxyphenyl)urea (11 b)

Yield 82% as yellow solid, m.p 257–260 °C. **¹HNMR (400 MHz, DMSO-d₆)** δ : 2.36–2.39 (t, 2H, CH₂CO, $J=8$ Hz), 2.89 (s, 3H, CH₃), 3.47–3.52 (q, 2H, CH₂NH, $J=8$ Hz), 3.72 (s, 3H, OCH₃), 6.47–6.49 (m, 1H, aromatic H₄''), 7.11–7.13 (d, 2H, aromatic H₅'', H₆'', $J=8$ Hz), 7.17–7.19 (d, 2H, aromatic H₂', H₆', $J=8$ Hz), 7.37 (s, 1H, aromatic H₂''), 7.49–7.52 (d, 2H, aromatic H₃', H₅', $J=8$ Hz), 8.12 (s, 1H, NH, exchangeable by D₂O), 8.26 (s, 1H, pyrimidine H), 9.09, 10.99, 11.12 ($s \times 3$, 3H, NH $\times 3$, exchangeable by D₂O). **MS: m/z (%)**: 535 (M⁺, 15%), 537 (M⁺+2, 8%), 93 (100%). **Anal. Calcd. For C₂₅H₂₅N₇O₅S**: C 56.06, H 4.70, N 18.31, S 5.99; Found: C 56.14, H 4.88, N 18.49, S 6.07.

5.1.12.3. 1-(4-(6-((3-(hydroxyamino)-3-oxopropyl)carbamoyl)-5-methylthieno[2,3-d]pyrimidin-4-ylamino)phenyl)-3-(3-(trifluoromethyl)phenyl)urea (11c)

Yield 79% as brown solid, m.p 281 °C. **¹HNMR (400 MHz, DMSO-d₆)** δ : 2.28–2.32 (t, 2H, CH₂CO, $J=8$ Hz), 2.90 (s, 3H, CH₃), 2.60 (s, 1H, OH, exchangeable by D₂O), 3.45–3.48 (m, 2H, CH₂NH), 7.22–7.24 (d, 1H, aromatic H₂', $J=8$ Hz), 7.31–7.33 (d, 1H, aromatic H₆', $J=8$), 7.45–7.49 (t, 1H, aromatic H₅', $J=8$ Hz), 7.53–7.55 (d, 1H, aromatic H₅'', $J=8$ Hz), 7.73–7.75 (d, 1H, aromatic H₃', $J=8$ Hz), 7.95 (s, 1H, aromatic H₄''), 8.13 (s, 1H, aromatic H₆''), 8.23 (s, 1H, aromatic H₂''), 8.35 (s, 1H, NH, exchangeable by D₂O), 8.51 (s, 1H, pyrimidine H), 9.00, 11.2, 11.5 ($s \times 3$, 3H, NH $\times 3$, exchangeable by D₂O). **MS: m/z (%)**: 575 (M⁺+2, 22%), 573 (M⁺, 52%), 140 (100%). **Anal. Calcd. For C₂₅H₂₂F₃N₇O₄S**: C 52.35, H 3.87, N 17.09, S 5.59; Found: C 52.48, H 3.95, N 17.31, S 5.48.

5.1.12.4. *N*-(3-(hydroxyamino)-3-oxopropyl)-5-methyl-4-(phenylamino)thieno[2,3-d]pyrimidine-6-carboxamide (19b). Yield 70% as yellow solid, m.p 267–270 °C. ¹HNMR (400 MHz, CDCl₃) δ: 2.17–2.21 (t, 2H, CH₂CO, *J* = 8 Hz), 2.90 (s, 3H, CH₃), 3.36–3.40 (t, 2H, CH₂NH, *J* = 8 Hz), 7.12–7.16 (t, 1H, aromatic H₄', *J* = 8 Hz), 7.36–7.40 (t, 2H, aromatic H₃', H₅', *J* = 8 Hz), 7.64–7.66 (d, 2H, aromatic H₂', H₆', *J* = 8 Hz), 8.45 (s, 1H, pyrimidine H), 8.49, 8.53, 8.84 (s × 3, 3H, NH × 3, exchangeable by D₂O), 10.30 (s, 1H, OH, exchangeable by D₂O). ¹³C NMR (DMSO-d₆, 400 MHz) δ: 16.20, 37.29, 37.73, 123.37, 124.39, 128.94, 139.36, 142.88, 154.50, 157.14, 159.06, 166.31, 173.12, 176.50. **MS: *m/z* (%)**: 373 (M⁺+2, 22%), 371 (M⁺, 41%), 309 (100%). **Anal. Calcd. For C₁₇H₁₇N₅O₃S**: C 54.97, H 4.61, N 18.86, S 8.63; Found: C 55.16, H 4.89, N 18.72, S 8.75.

5.1.12.5. 4-(4-chlorophenylamino)-*N*-(3-(hydroxyamino)-3-oxopropyl)-5-methylthieno[2,3-d]pyrimidine-6-carboxamide (19c). Yield 75% as yellowish orange solid, m.p 282 °C. ¹HNMR (400 MHz, DMSO-d₆) δ: 1.04–1.08 (t, 2H, CH₂CO, *J* = 8 Hz), 2.09 (s, 3H, CH₃), 3.38–3.46 (m, 2H, CH₂NH), 4.40 (s, 1H, NH, exchangeable by D₂O), 7.41–7.43 (d, 2H, aromatic H₃', H₅', *J* = 8 Hz), 7.69–7.71 (d, 2H, aromatic H₂', H₆', *J* = 8 Hz), 8.46 (s, 1H, pyrimidine H), 8.67, 8.90 (s × 2, 2H, NH × 2, exchangeable by D₂O). **MS: *m/z* (%)**: 407 (M⁺+2, 66%), 406 (M⁺+1, 41%), 405 (M⁺, 19%), 352 (100%). **Anal. Calcd. For C₁₇H₁₆ClN₅O₃S**: C 50.31, H 3.97, N 17.26, S 7.90; Found: C 50.49, H 4.18, N 17.40, S 7.86.

5.1.12.6. 4-(3-chloro-4-fluorophenylamino)-*N*-(3-(hydroxyamino)-3-oxopropyl)-5-methylthieno[2,3-d]pyrimidine-6-carboxamide (19d). Yield 78% as yellow solid, m.p. 276 °C. ¹HNMR (400 MHz, DMSO-d₆) δ: 2.09 (s, 1H, OH, exchangeable by D₂O), 2.18–2.22 (t, 2H, CH₂CO, *J* = 8 Hz), 2.89 (s, 3H, CH₃), 3.42–3.47 (m, 2H, CH₂NH), 7.39–7.44 (t, 1H, aromatic H₅', *J* = 8 Hz), 7.62–7.64 (m, 1H, aromatic H₂''), 7.90–7.93 (dd, 1H, aromatic H₆', *J* = 4 Hz, 8 Hz), 8.47–8.48 (m, 2H, pyrimidine H, NH exchangeable by D₂O), 8.78 (s, 1H, NH, exchangeable by D₂O). **MS: *m/z* (%)**: 423 (M⁺, 49%), 420 (M⁺+2, 10%), 76 (100%). **Anal. Calcd. For C₁₇H₁₅ClFN₅O₃S**: C 48.17, H 3.57, N 16.52, S 7.57; Found: C 48.40, H 3.71, N 16.80, S 7.63.

5.1.12.7. 1-(4-(6-((4-(hydroxyamino)-4-oxobutyl)carbamoyl)-5-methylthieno[2,3-d]pyrimidin-4-ylamino)phenyl)-3-phenylurea (12a). Yield 69% as yellow solid, m.p 219 °C. ¹HNMR (400 MHz, DMSO-d₆) δ: 1.77–1.84 (m, 2H, CH₂CH₂CH₂), 2.18–2.22 (t, 2H, CH₂CO, *J* = 8 Hz), 2.88 (s, 3H, CH₃), 3.26–3.35 (m, 2H, CH₂NH), 6.90–6.94 (t, 1H, aromatic H₄'', *J* = 8 Hz), 7.23–7.27 (t, 2H, aromatic H₃'', H₅'', *J* = 8 Hz), 7.40–7.42 (d, 2H, aromatic H₂', H₆', *J* = 8 Hz), 7.47–7.49 (d, 2H, aromatic H₃', H₅', *J* = 8 Hz), 7.53–7.55 (d, 2H, aromatic H₂'', H₆'', *J* = 8 Hz), 8.22, 8.28 (s × 2, 2H, NH × 2, exchangeable by D₂O), 8.36 (s, 1H, pyrimidine H), 8.41, 9.01, 9.50 (s × 3, 3H, NH × 3, exchangeable by D₂O), 9.98 (s, 1H, OH, exchangeable by D₂O). **MS: *m/z* (%)**: 519 (M⁺, 27%), 516 (M⁺+3, 20%), 432 (100%). **Anal. Calcd. For C₂₅H₂₅N₇O₄S**: C 57.79, H 4.85, N 18.87, S 6.17; Found: C 57.80, H 4.82, N 18.89, S 6.16

5.1.12.8. 1-(4-(6-((4-(hydroxyamino)-4-oxobutyl)carbamoyl)-5-methylthieno[2,3-d]pyrimidin-4-ylamino)phenyl)-3-(3-methoxyphenyl)urea (12b). Yield 67% as orange solid, m.p 231–233 °C. ¹HNMR (400 MHz, DMSO-d₆) δ: 1.71–1.80 (m, 2H, CH₂CH₂CH₂), 2.19–2.22 (t, 2H, CH₂CO, *J* = 8 Hz), 2.87 (s, 3H, CH₃), 3.31–3.41 (m, 2H, CH₂NH), 3.72 (s, 3H, OCH₃), 6.46–7.48 (d, 1H, aromatic H₄'', *J* = 8 Hz), 7.09–7.13 (m, 2H, aromatic H₅'', H₆''), 7.30–7.32 (d, 2H, aromatic H₂', H₆', *J* = 8 Hz), 7.33 (s, 1H, aromatic H₂''), 7.44–7.46 (d, 2H, aromatic H₃', H₅', *J* = 8 Hz), 8.18 (s, 1H, NH, exchangeable by

D₂O), 8.30 (s, 1H, pyrimidine H), 8.52, 9.53, 10.76, 10.86 (s × 4, 3H, NH × 3, exchangeable by D₂O). **MS: *m/z* (%)**: 549 (M⁺, 28%), 547 (M⁺+2, 16%), 221 (100%). **Anal. Calcd. For C₂₆H₂₇N₇O₅S**: C 56.82, H 4.95, N 17.84, S 5.83; Found: C 57.04, H 5.19, N 17.71, S 5.96. **FT-IR (ú max, cm⁻¹)**: 3441 (OH broad), 3317 (NH stretch), 2958 (CH aromatic), 2931–2835 (CH aliphatic), 1708 (C=O), 1643 (C=O amide), 1612 (NH bend).

5.1.12.9. 1-(4-(6-((4-(hydroxyamino)-4-oxobutyl)carbamoyl)-5-methylthieno[2,3-d]pyrimidin-4-ylamino)phenyl)-3-(3-(trifluoromethyl)phenyl)urea (12c). Yield 72% as yellow solid, m.p. 215–217 °C. ¹HNMR (400 MHz, DMSO-d₆) δ: 1.75–1.84 (m, 2H, CH₂CH₂CH₂), 2.09–2.24 (m, 2H, CH₂CO), 2.88 (s, 3H, CH₃), 3.38–3.45 (m, 2H, CH₂NH), 7.22–7.25 (t, 1H, aromatic H₆', *J* = 8 Hz), 7.35–7.37 (d, 1H, aromatic H₂', *J* = 8 Hz), 7.45–7.47 (d, 1H, aromatic H₅', *J* = 8 Hz), 7.49–7.51 (d, 1H, aromatic H₃', *J* = 8 Hz), 7.54–7.56 (d, 1H, aromatic H₄''), 7.67–7.73 (dd, 1H, aromatic H₆'', *J* = 8 Hz, 16 Hz), 8.09–8.12 (d, 1H, aromatic H₅''), 8.32 (s, 1H, aromatic H₂''), 8.41 (s, 1H, pyrimidine H), 8.53, 9.44, 10.53, 10.85, 10.93, (s × 5, 5H, NH × 5, exchangeable by D₂O), 11.39 (s, 1H, OH, exchangeable by D₂O). **MS: *m/z* (%)**: 587 (M⁺, 64%), 255 (100%), 205 (93%). **Anal. Calcd. For C₂₆H₂₄F₃N₇O₄S**: C 53.15, H 4.12, N 16.69, S 5.46; Found: C 53.31, H 4.26, N 16.83, S 5.60.

5.1.12.10. *N*-(4-(hydroxyamino)-4-oxobutyl)-5-methyl-4-(phenylamino)thieno[2,3-d]pyrimidine-6-carboxamide (20b). Yield 75% as yellow solid, m.p 205 °C. ¹HNMR (400 MHz, CDCl₃) δ: 1.78 (m, 2H, CH₂CH₂CH₂), 2.06 (m, 2H, CH₂CO), 2.88 (s, 3H, CH₃), 3.25–3.36 (m, 2H, CH₂NH), 7.16–7.65 (m, 5H, aromatic H), 8.45–8.49 (m, 2H, pyrimidine H, NH), 8.77 (s, 1H, NH, exchangeable by D₂O). **MS: *m/z* (%)**: 385 (M⁺, 12%), 383 (M⁺+2, 5%), 308 (100%). **Anal. Calcd. For C₁₈H₁₉N₅O₃S**: C 56.09, H 4.97, N 18.17, S 8.32; Found: C 56.24, H 4.89, N 18.40, S 8.45. **FT-IR (ú max, cm⁻¹)**: 3452, 3232 (2 × NH stretch), 3410 (OH/NH broad), 3059–2970 (CH aromatic), 2931–2823 (CH aliphatic), 1647 (C=O amide), 1608 (NH bend).

5.1.12.11. 4-(4-chlorophenylamino)-*N*-(4-(hydroxyamino)-4-oxobutyl)-5-methylthieno[2,3-d]pyrimidine-6-carboxamide (20c). Yield 78% as yellow solid, m.p 212 °C. ¹HNMR (400 MHz, DMSO-d₆) δ: 1.65 (s, 1H, OH, exchangeable by D₂O), 1.69–1.76 (m, 2H, CH₂CH₂CH₂), 2.06–2.09 (t, 2H, CH₂CO, *J* = 8 Hz), 2.88 (s, 3H, CH₃), 3.23–3.27 (q, 2H, CH₂NH, *J* = 8 Hz), 7.41–7.43 (d, 2H, aromatic H₂', H₆', *J* = 8 Hz), 7.69–7.71 (d, 1H, aromatic H₃', H₅', *J* = 8 Hz), 8.46 (s, 1H, pyrimidine H), 8.50, 8.64, 9.63 (s × 3, 3H, NH × 3, exchangeable by D₂O). ¹³C NMR (DMSO-d₆, 400 MHz) δ: 16.25, 22.69, 25.65, 36.32, 122.16, 124.90, 128.77, 129.29, 147.56, 147.94, 131.70, 150.08, 154.32, 160.59, 162.43, 166.44. **MS: *m/z* (%)**: 419 (M⁺, 23%), 421 (M⁺+1, 31%), 98 (100%). **Anal. Calcd. For C₁₈H₁₈ClN₅O₃S**: C 51.49, H 4.32, N 16.68, S 7.64; Found: C 51.63, H 4.58, N 16.79, S 7.58.

5.1.12.12. 4-(3-chloro-4-fluorophenylamino)-*N*-(4-(hydroxyamino)-4-oxobutyl)-5-methylthieno[2,3-d]pyrimidine-6-carboxamide (20d). Yield 80% as brown solid, m.p 244–246 °C. ¹HNMR (400 MHz, DMSO-d₆) δ: 1.71–1.76 (m, 2H, CH₂CH₂CH₂), 2.09–2.13 (t, 2H, CH₂CO, *J* = 8 Hz), 2.87 (s, 3H, CH₃), 3.22–3.28 (q, 2H, CH₂NH, *J* = 8 Hz), 7.40–7.44 (t, 1H, aromatic H₅', *J* = 8 Hz), 7.63–7.65 (m, 1H, aromatic H₂''), 7.91–7.93 (d, 1H, aromatic H₆', *J* = 8 Hz), 8.47 (s, 1H, pyrimidine H), 9.43 (s, 1H, NH, exchangeable by D₂O). **MS: *m/z* (%)**: 439 (M⁺+2, 26%), 437 (M⁺, 100%), 436 (M⁺+1, 84%). **Anal. Calcd. For C₁₈H₁₇ClFN₅O₃S**: C 49.37, H 3.91, N 15.99, S 7.32; Found: C 49.60, H 4.04, N 16.12, S 7.30.

5.2. Biological evaluation

5.2.1. *In vitro* EGFR and VEGFR-2 tyrosine kinase inhibitory activity

In vitro enzyme inhibition determination for the synthesised compounds was carried out in Thermo Fischer Scientific, Madison, WI, USA (SelectScreenServices@thermofisher.com). The EGFR and VEGFR-2 tyrosine kinase % inhibitory activity at a single-dose concentration of 10 μ M was performed initially then representative compounds were evaluated at single-dose concentrations of (0.1 nM, 1 nM, 10 nM, 100 nM, 1 μ M) using ZYLTE technology. A fluorescence-based, coupled-enzyme format is employed in the biochemical assay and depends on the sensitivity of proteolytic cleavage to non-phosphorylated and phosphorylated peptides. Then IC₅₀ values for selected compounds were determined by GraphPad Prism at Misr international university.

5.2.2. *In vitro* HDAC inhibitory activity

5.2.2.1. Materials and methods. The HDAC inhibitory activity was carried out at BPS Bioscience (www.bpsbioscience.com). All of the synthesised compounds were tested at 10 μ M for their inhibitory percent against HDAC6. HDAC6 (BPS#50006), HDAC substrate 3 (BPS#50037), HDAC Assay Buffer (BPS catalogue number 50031) and HDAC Assay Developer (BPS catalogue number 50030) was used in testing. TSN is also used as a reference compound purchased from Selleckcom.com (#S1045).

5.2.2.2. HDAC6 inhibitory activity assay protocols. All compounds are dissolved in DMSO. Serial dilutions of the compounds were carried out with 10% DMSO in HDAC assay buffer and 5 μ l of the dilution was mixed to a 50 μ l reaction so that the final concentration of DMSO is 1% in all of the reactions. Duplicate enzymatic reactions were conducted at 37 °C in a 50 μ l mixture containing HDAC assay buffer, 5 μ g BSA, HDAC substrate 3, HDAC6 (catalogue# 50006), and a test compound (10 μ M) for 30 to 60 min. 50 μ l of 2 \times HDAC Developer was added to each well after enzymatic reaction, and the plate was incubated at room temperature for another 15 min. Fluorescence intensity was measured using a Tecan Infinite M1000 microplate reader at an excitation of 360 nm and an emission of 460 nm

5.2.2.3. Data analysis. Duplicates of HDAC activity assays were performed at each concentration. Analysis of the fluorescent intensity data was performed using the Graphpad Prism computer software., the % activity was calculated according to the equation: % activity = $(F - F_b) / (F_t - F_b)$, where F = the fluorescent intensity in each data set in the presence of the compound, F_t = the fluorescent intensity in each data set, defined as 100% activity in the absence of the compound, F_b = the fluorescent intensity in each data set, defined as 0% activity in the absence of HDAC.

5.2.3. *In vitro* anticancer activity

All of the synthesised compounds (20) were submitted to NCI and selected for *in vitro* anticancer assay against a panel of 60 cancer cell lines. The methodology of assay and calculations is as reported [54,55].

Acknowledgement

The authors are very grateful to the National Cancer Institute 'NCI', Maryland, USA for the *in vitro* anticancer screening of all the

synthesized compounds and would like to thank BPS Bioscience and Thermo Fischer Scientific for performing the HDAC inhibitory assay and Kinase assays for all of the synthesized compounds, respectively.

Disclosure statement

No potential conflict of interest was reported by the author(s).

References

- Cai X, Zhai H-X, Wang J, et al. Discovery of 7-(4-(3-ethynylphenylamino)-7-methoxyquinazolin-6-yloxy)-N-hydroxyheptanamide (CUDc-101) as a potent multi-acting HDAC, EGFR, and HER2 inhibitor for the treatment of cancer. *J Med Chem* 2010;53:2000–9.
- Falkenberg KJ, Johnstone RW. Histone deacetylases and their inhibitors in cancer, neurological diseases and immune disorders. *Nat Rev Drug Discov* 2014;13:673–91.
- Lu H, Chen Y-d, Yang B, You Q-d. Design, synthesis and biological evaluation of novel histone deacetylase inhibitors based on virtual screening. *Acta Pharmaceutica Sinica B* 2011;1:240–7.
- Depetter Y, Geurs S, De Vreese R, et al. Selective pharmacological inhibitors of HDAC6 reveal biochemical activity but functional tolerance in cancer models. *Int J Cancer* 2019;145:735–47.
- Yang F, Zhao N, Ge D, Chen Y. Next-generation of selective histone deacetylase inhibitors. *RSC Advances* 2019;9:19571–83.
- Yang Z, Wang T, Wang F, et al. Discovery of Selective Histone Deacetylase 6 Inhibitors Using the Quinazoline as the Cap for the Treatment of Cancer. *J Med Chem* 2016;59:1455–70.
- Yang W, Li L, Ji X, et al. Design, synthesis and biological evaluation of 4-anilinothieno[2,3-d]pyrimidine-based hydroxamic acid derivatives as novel histone deacetylase inhibitors. *Bioorg Med Chem* 2014;22:6146–55.
- Guha M. HDAC inhibitors still need a home run, despite recent approval. *Nat Rev Drug Discov* 2015;14:225–6.
- Suraweera A, O'Byrne KJ, Richard DJ. Combination therapy with histone deacetylase inhibitors (HDACi) for the treatment of cancer: achieving the full therapeutic potential of HDACi. *Front Oncol* 2018;8:92.
- Witta SE, Dziadziuszko R, Yoshida K, et al. ErbB-3 expression is associated with E-cadherin and their coexpression restores response to gefitinib in non-small-cell lung cancer (NSCLC). *Ann Oncol* 2009;20:689–695.
- Aggarwal R, Thomas S, Pawlowska N, et al. Inhibiting histone deacetylase as a means to reverse resistance to angiogenesis inhibitors: phase I study of abexinostat plus pazopanib in advanced solid tumor malignancies. *J Clin Oncol* 2017;35:1231–1239.
- Zang J, Liang X, Huang Y, et al. Discovery of novel pazopanib-based HDAC and VEGFR dual inhibitors targeting cancer epigenetics and angiogenesis simultaneously. *J Med Chem* 2018;61:5304–5322.
- Ding C, Li D, Wang Y-W, et al. Discovery of ErbB/HDAC inhibitors by combining the core pharmacophores of HDAC inhibitor vorinostat and kinase inhibitors vandetanib, BMS-690514, neratinib, and TAK-285. *Chinese Chem Lett* 2017;28:1220–1227.

14. Peng FW, Xuan J, Wu TT, et al. Design, synthesis and biological evaluation of N-phenylquinazolin-4-amine hybrids as dual inhibitors of VEGFR-2 and HDAC. *Eur J Med Chem* 2016;109:1–12.
15. Mghwary AES, Gedawy EM, Kamal AM, Abuel-Maaty SM. Novel thienopyrimidine derivatives as dual EGFR and VEGFR-2 inhibitors: design, synthesis, anticancer activity and effect on cell cycle profile. *J Enzyme Inhib Med Chem* 2019;34:838–852.
16. Wedge SR, Ogilvie DJ, Dukes M, et al. ZD6474 inhibits vascular endothelial growth factor signaling, angiogenesis, and tumor growth following oral administration. *Cancer Res* 2002;62:4645–4655.
17. Morabito A, Piccirillo MC, Falasconi F, et al. Vandetanib (ZD6474), a dual inhibitor of vascular endothelial growth factor receptor (VEGFR) and epidermal growth factor receptor (EGFR) tyrosine kinases: current status and future directions. *The Oncologist* 2009;14:378–390.
18. Yang W, Li L, Wang Y, et al. Design, synthesis and biological evaluation of isoquinoline-based derivatives as novel histone deacetylase inhibitors. *Bioorg Med Chem* 2015;23:5881–5890.
19. Butler KV, Kalin J, Brochier C, et al. Rational design and simple chemistry yield a superior, neuroprotective HDAC6 inhibitor, tubastatin A. *J Am Chem Soc* 2010;132:10842–10846.
20. Wang F, Zheng L, Yi Y, et al. SKLB-23bb, A HDAC6-Selective Inhibitor. Exhibits Superior and Broad-Spectrum Antitumor Activity via Additionally Targeting Microtubules, *Molecular Cancer Therapeutics* 2018;17:763–775.
21. Dewal MB, Wani AS, Vidailac C, et al. Thieno[2,3-d]pyrimidinedione derivatives as antibacterial agents. *Eur J Med Chem* 2012;51:145–153.
22. Adel M, Serya RAT, Lasheen DS, Abouzid KAM. Identification of new pyrrolo[2,3-d]pyrimidines as potent VEGFR-2 tyrosine kinase inhibitors: Design, synthesis, biological evaluation and molecular modeling. *Bioorg Chem* 2018;81:612–629.
23. Dai Y, Hartandi K, Ji Z, et al. Discovery of N-(4-(3-amino-1H-indazol-4-yl)phenyl)-N'-(2-fluoro-5-methylphenyl)urea (ABT-869), a 3-aminoindazole-based orally active multitargeted receptor tyrosine kinase inhibitor. *J Med Chem* 2007;50:1584–1597.
24. Suzuki T KM, Sawada H, Imai E, et al. Design, synthesis, and biological activity of a novel series of human sirtuin-2-selective inhibitors. *J Med Chem* 2012;55:5760–5773.
25. Wu CH, Coumar MS, Chu CY, et al. Design and synthesis of tetrahydropyridothieno[2,3-d]pyrimidine scaffold based epidermal growth factor receptor (EGFR) kinase inhibitors: the role of side chain chirality and Michael acceptor group for maximal potency. *J Med Chem* 2010;53:7316–7326.
26. Kassab SE, Mowafy S, Alserw AM, et al. Structure-based design generated novel hydroxamic acid based preferential HDAC6 lead inhibitor with on-target cytotoxic activity against primary choroid plexus carcinoma. *J Enzyme Inhib Med Chem* 2019;34:1062–1077.
27. Zuo M, Zheng Y-W, Lu S-M, et al. Synthesis and biological evaluation of N-aryl salicylamides with a hydroxamic acid moiety at 5-position as novel HDAC-EGFR dual inhibitors. *Bioorg Med Chem* 2012;20:4405–4412.
28. G. Hoelzemann, D. Dorsch, H. Greiner, C. Amendt, F. Zenke, Alkoxy-thienopyrimidines as tgf-beta receptor kinase modulators, in, Google Patents, 2010.
29. Voynikov Y, Stavrov G, Tencheva J, Peikov P. Novel Leucine Derived Amides of Theophylline-7-acetic Acid. *Comptes Rendus de L'Académie Bulgare Des Sciences: sciences Mathématiques et Naturelles* 2013;66:1399.
30. Ghith A, Youssef KM, Ismail NSM, Abouzid KAM. Design, synthesis and molecular modeling study of certain VEGFR-2 inhibitors based on thienopyrimidine scaffold as cancer targeting agents. *Bioorg Chem* 2019;83:111–128.
31. Zhang Y, Chen Y, Zhang D, et al. Discovery of novel potent VEGFR-2 inhibitors exerting significant antiproliferative activity against cancer cell lines. *J Med Chem* 2018;61:140–157.
32. Liu Z, Qi L, Li Y, et al. VEGFR2 regulates endothelial differentiation of colon cancer cells. *BMC Cancer* 2017;17:593.
33. Kris MG, Natale RB, Herbst RS, et al. Efficacy of gefitinib, an inhibitor of the epidermal growth factor receptor tyrosine kinase, in symptomatic patients with non-small cell lung cancer: a randomized trial. *JAMA* 2003;290:2149–2158.
34. Badalian G, Derecskei K, Szendroi A, et al. EGFR and VEGFR2 protein expressions in bone metastases of clear cell renal cancer. *Anticancer Res* 2007;27:889–894.
35. Barker FG, 2nd, Simmons ML, Chang SM, et al. EGFR overexpression and radiation response in glioblastoma multiforme. *Int J Radiation Oncol Biol Phys* 2001;51:410–418.
36. Park JH, Liu Y, Lemmon MA, Radhakrishnan R. Erlotinib binds both inactive and active conformations of the EGFR tyrosine kinase domain. *Biochem J* 2012;448:417–423.
37. Sobhy MK, Mowafy S, Lasheen DS, et al. 3D-QSAR pharmacophore modelling, virtual screening and docking studies for lead discovery of a novel scaffold for VEGFR 2 inhibitors: Design, synthesis and biological evaluation. *Bioorg Chem* 2019;89:102988.
38. Aziz MA, Serya RA, Lasheen DS, et al. Discovery of potent VEGFR-2 inhibitors based on furopyrimidine and thienopyrimidine scaffolds as cancer targeting agents. *Scientific Rep* 2016;6:24460.
39. Miyake Y, Keusch JJ, Wang L, et al. Structural insights into HDAC6 tubulin deacetylation and its selective inhibition. *Nature Chem Biol* 2016;12:748–754.
40. Alsawalha M, Rao Bolla S, Kandakatla N, et al. Molecular docking and ADMET analysis of hydroxamic acids as HDAC2 inhibitors. *Bioinformation* 2019;15:380–387.
41. Palm K, Stenberg P, Luthman K, Artursson P. Polar molecular surface properties predict the intestinal absorption of drugs in humans. *Pharmaceut Res* 1997;14:568–571.
42. Egan WJ, Merz KM, Jr., Baldwin JJ. Prediction of drug absorption using multivariate statistics. *J Med Chem* 2000;43:3867–3877.
43. Hafez HN, El-Gazzar ABA. Design and synthesis of 3-pyrazolyl-thiophene, thieno[2,3-d]pyrimidines as new bioactive and pharmacological activities. *Bioorg Med Chem Lett* 2008;18:5222–5227.
44. Grinev AN, Kaplina NV. Transformations of 5-methyl-6-carbetoxy-3,4-dihydrothieno-[2,3-d]pyrimidine for synthesis of 4-methoxy-, 4-alkylamino-, and other derivatives of thieno[2,3-d]pyrimidine. *Chem Heterocyclic Comp* 1985;21:767–770.
45. J. Das, J. Hynes, K. Leftheris, S. Lin, S. T. Wroblewski, H. Wu, Phenyl-aniline substituted bicyclic compounds useful as kinase inhibitors, in: US7419978, 2005.
46. Reddy LS, Chandran SK, George S, et al. Crystal structures of N-Aryl-N'-4-nitrophenyl ureas: molecular conformation and weak interactions direct the strong hydrogen bond synthon. *Crystal Growth Design* 2007;7:2675–2690.

47. Roice M, Christensen SF, Meldal M. ULTRAMINE: a high-capacity polyethylene-imine-based polymer and its application as a scavenger resin. *Chemistry* 2004;10:4407–4415.
48. Uno M, Ban HS, Nabeyama W, Nakamura H. de novo design and synthesis of N-benzylanilines as new candidates for VEGFR tyrosine kinase inhibitors. *Org Biomol Chem* 2008;6: 979–981.
49. Shi L, Wu TT, Wang Z, et al. Discovery of quinazolin-4- amines bearing benzimidazole fragments as dual inhibitors of c-Met and VEGFR-2. *Bioorg Med Chem* 2014;22: 4735–4744.
50. K. Abouzid, E. Zaglol El-Razaz, R. T Serya, Thienopyrimidine compounds as tyrosine kinase inhibitors and anticancer agents, in: Egyptian patent office 545/2017, app date: 28-3-2017.
51. Muthu K, Bariwal J, Vyas V, et al. Novel Dual Use of Formamide-POCl₃ Mixture for the Efficient, One-Pot Synthesis of Condensed 2H -Pyrimidin-4-amine Libraries Under Microwave Irradiation. *Syn Commun* 2013;43:719–727.
52. Kotaiah Y, Harikrishna N, Nagaraju K, Venkata Rao C. Synthesis and antioxidant activity of 1,3,4-oxadiazole tagged thieno[2,3-d]pyrimidine derivatives. *Eur J Med Chem* 2012; 58:340–345.
53. *Scifinderⁿ*, version 2020, Chemical Abstracts Service; RN 1029777-26-1 (accessed 7/7/2020).
54. Alley MC, Scudiero DA, Monks A, et al. Feasibility of drug screening with panels of human tumor cell lines using a microculture tetrazolium assay. *Cancer Res* 1988;48:589–601.
55. Shoemaker RH. The NCI60 human tumour cell line anti-cancer drug screen. *Nature Rev Cancer* 2006;6:813–823.